PB81-116014

Modeling the Evolution of the Convective Planetary Boundary Layer

Illinois Univ. at Urbana-Champaign

Prepared for

National Severe Storms Lab.
Norman, OK

Feb 80

U.S. Department of Commerce
National Technical Information Service
NTIS.

80091904

Final Report
NOAA Grant No. 04-7-022-44026

PB81-116014

Modeling the Evolution of the Convective Planetary Boundary Layer

by

Wen-Yih Sun* and Yoshi Ogura

Laboratory for Atmospheric Research
University of Illinois
Urbana, IL 61801

(revised manuscript)

February 1980

*Present affiliation: Department of Geosciences, Purdue University
West Lafayette, Indiana 47907

REPRODUCED BY
NATIONAL TECHNICAL
INFORMATION SERVICE
U.S. DEPARTMENT OF COMMERCE
SPRINGFIELD, VA 22161

NOAA FORM 25-13 (1-78)

BIBLIOGRAPHIC DATA SHEET

U. S. DEPARTMENT OF COMMERCE
NATIONAL OCEANIC AND ATMOSPHERIC ADMINISTRATION

1. NOAA ACCESSION NUMBER	2.	3. RECIPIENT'S ACCESSION NUMBER
NOAA-80091904		PB81 116014

4. TITLE AND SUBTITLE
Modeling the Evolution of the Convective Planetary Boundary Layer

5. REPORT DATE
Feb 1980

6.

7. AUTHOR(S)
Wen-Yih Sun and Yoshi Ogura

8. REPORT NO.

9. PERFORMING ORGANIZATION NAME AND ADDRESS
Illinois University, Urbana 61801,
Laboratory for Atmospheric Research

10. PROJECT/TASK NO.

11. CONTRACT/GRANT NO.
04-7-022-44026

12. SPONSORING ORGANIZATION NAME AND ADDRESS
NOAA, National Severe Storms Laboratory,
Norman, OK 73069

13. TYPE OF REPORT AND PERIOD COVERED
Final Report

14.

15. PUBLICATION REFERENCE
Illinois University Laboratory for Atmospheric Research Final Report to NOAA, National Severe Storms Laboratory, February 1980. 52 p, 21 fig, 1 tab, 23 ref.

16. ABSTRACT
The Level 3 turbulence closure model proposed by Mellor and Yamada (1974) is modified (a) to incorporate the formulations for the turbulence third order moments and pressure terms proposed by Zeman and Lumley (1976) and (b) to introduce turbulence length scales which depend upon the stratification of the atmosphere. The vertical heat and moisture fluxes and the temperature-humidity covariance are determined from differential equations. The model includes two other differential equations, one for the turbulence kinetic energy and the other for virtual potential temperature variance. All other turbulence variables are determined from algebraic equations. The model is used to simulate the daytime evolution of the planetary boundary layer observed on day 33 of the Wangara boundary layer experiment. The calculated vertical profiles of the mean wind, temperature and humidity are found to be in good agreement with the observations. The calculated vertical distributions of turbulence variables, including kinetic energy, temperature variance, heat and moisture fluxes, temperature and moisture variance, molecular dissipation, and some third order moments, compare favorably with those estimated from other numerical models, aircraft observations and laboratory experiments. (Author)

17. KEY WORDS AND DOCUMENT ANALYSIS

17A. DESCRIPTORS
*Turbulence, *Boundary layer, *Mathematical models, Temperature, Humidity

17B. IDENTIFIERS/OPEN-ENDED TERMS
Planetary boundary layer

17C. COSATI FIELD/GROUP
4A

18. AVAILABILITY STATEMENT
Released for distribution:
Elaine L. Downs

19. SECURITY CLASS (This report)	21. NO. OF PAGES
UNCLASSIFIED	
20. SECURITY CLASS (This report)	**22. PRICE**
UNCLASSIFIED	

NOAA FORM 25-13 (1-78) SUPERSEDES ALL PREVIOUS EDITIONS.

ABSTRACT

The Level 3 turbulence closure model proposed by Mellor and Yamada (1974) is modified (a) to incorporate the formulations for the turbulence third order moments and pressure terms proposed by Zeman and Lumley (1976) and (b) to introduce turbulence length scales which depend upon the stratification of the atmosphere. The vertical heat and moisture fluxes and the temperature-humidity covariance are determined from differential equations. The model includes two other differential equations, one for the turbulence kinetic energy and the other for virtual potential temperature variance. All other turbulence variables are determined from algebraic equations

The model is used to simulate the daytime evolution of the planetary boundary layer observed on day 33 of the Wangara boundary layer experiment. The calculated vertical profiles of the mean wind, temperature and humidity are found to be in good agreement with the observations. The calculated vertical distributions of turbulence variables, including kinetic energy, temperature variance, heat and moisture fluxes, temperature and moisture variance, molecular dissipation, and some third order moments, compare favorably with those estimated from other numerical models, aircraft observations and laboratory experiments.

1. Introduction

In recent years several authors have developed what we may call high-order turbulence closure model for inhomogeneous and anisotropic tubulence. The real equations governing the first moments include turbulence second moments such as the Reynolds stresses and the turbulent heat and moisture fluxes. The equations governing the second moments include new unknown variables, chiefly the third moments and pressure terms, and so on. The second-order model aims at closing this infinite set of equations at the second moments, by relating all third moments and pressure terms to the first and second moments. Hanjalic and Launder (1972) proposed a eddy-damped quasi-Gaussian approximation to the third moments. The method has been extended by Lumley and Khajeh-Nouri (1974) and successfully applied to thermal convection by Zeman and Lumley (1976) (which will be referred to as ZL hereafter) and Lumley et al. (1978).

André et al. (1976a,b) proposed a third-order model with a clipping approximation. In this model quasi-normal theory is modified by limiting the growth of third moments using generalized Schwarz's inequalities. They applied their theory to the shear-free, horizontally homogeneous penetrative convection observed by Willis and Deardorff (1974) in their laboratory experiment. The model successfully reproduced the measured vertical variations of mean temperature, turbulence heat flux, eddy kinetic energy and temperature variance, as well as third moments such as the vertical flux of eddy kinetic energy. Later André et al. (1978) extended their model to include the effect of radiative heat transfer and simulated the 24-hour evolution of the mean and turbulent structures of the planetary boundary layer observed on Days 33-34 in the Wangara experiment in southeast Australia.

All of the above models are fairly complicated, even with approximations suitable for a horizontally homogeneous boundary layer in which moisture is not considered. The second-order model of ZL requires the solution of 12 prognostic differential equations in addition to the differential equations for the first moments. The third-order model for a moist planetary boundary layer proposed by André et al. (1978) requires the solution of 33 prognostic equations for turbulence variables. Mellor and Yamada (1974) presented an analysis which systematically simplifies the second-order closure model (that is, the Level 4 model in Mellor-Yamada's terminology) into the Level 3 model (which will be referred to as MY model hereafter). The Level 3 requires only two differential equations for a dry boundary layer.

The MY model has been applied by Yamada and Mellor (1975) to simulate the diurnal variations in the planetary boundary layer observed in the Wangara experiment. The gross behavior of the simulated boundary layer agrees well with the observations. However, the depth of the mixed layer is consistently underestimated, the downward heat flux at or near the top of the inversion is also underestimated in comparison with other observations and the temperature stratification in the main body of the mixed layer is slightly unstable instead of neutral as we might expect. André et al. (1976a,b) and ZL have pointed out that simple gradient type diffusion terms, such as those applied in MY and Wyngaard and Coté's model (1974), hereafter called WC, are inadequate to realistically represent the diffusion terms (third moments) in a convective boundary layer.

In this article we shall develop a turbulence model for a moist planetary boundary layer. This model is similar to MY. However, the formulations for the third moments and the pressure terms proposed by Zeman (1975) and ZL will be incorporated into the model. A turbulence length scale in a stably stratified atmosphere will also be introduced. Further, the vertical heat

flux, moisture flux and the temperature-humidity covariance will be determined from differential rather than from algebraic equations, in contrast to MY. The model will be used to simulate the evolution of the convective boundary layer observed during the period from 09 to 18 EST on Day 33 of the Wangara experiment. On this particular day ideal meteorological conditions occured; i.e., clear skies, very little horizontal advection of heat or moisture and lack of any frontal activity within 1000 km. Thus, many modelers have compared their results with these observations, including Deardorff (1974a,b), Wyngaard and Coté (1974), Pielke and Mahrer (1975), Yamada and Mellor (1975) and André et al. (1978).

However, the Wangara experiment does not provide directly measured turbulence data. We shall therefore compare the turbulence variables calculated from our model with data from other sources. One important source is the three-dimensional numerical experiment of Deardorff (1974a,b) in which a portion of the turbulence was explicitly calculated and only subgrid-scale turbulence was modeled by second-order closure approximations. Another source is direct aircraft or tethered balloon measurements in and above the planetary boundary layers over the various parts of the world and under different meteorological conditions. This includes measurements by Telford and Warner (1964) in New South Wales; by Lenschow and Johnson (1968) over a forested area in northeastern Wisconsin; by Lenschow (1970) over relatively flat terrain in eastern Colorado; by Lenschow (1974) over the Great Lakes; by Kaimal et al. (1976) over a flat site in northwestern Minnesota; by Caughey and Palmer (1979) at Ashchurch, Worchestershire; and by Wyngaard et al. (1978) during AMTEX (Air Mass Transformation Experiment) over the East China Sea. A third source for comparison data is the laboratory measurements of convective boundary layers performed by Willis and Deardorff (1974), and Ferriera (1978), even though the vertically varying mean flow is absent in these laboratory measurements.

2. The model equations

The governing equations for the mean variables in a quasi-horizontally homogeneous flow are

$$\frac{\partial U}{\partial t} = fV - fV_g + \frac{\partial}{\partial z}(-\overline{uw}) \tag{1}$$

$$\frac{\partial V}{\partial t} = -fU + fU_g + \frac{\partial}{\partial z}(-\overline{vw}) \tag{2}$$

$$\frac{\partial \Theta}{\partial t} = \frac{\partial}{\partial z}(-\overline{w\theta}) + \frac{f\Theta_o}{g}\left(V\frac{\partial U_g}{\partial z} - U\frac{\partial V_g}{\partial z}\right) \tag{3}$$

$$\frac{\partial R}{\partial t} = -\frac{\partial \overline{wr}}{\partial z} \tag{4}$$

where (U,V,0) and (u,v,w) are mean and fluctuating velocity vectors in the x (eastward), y (northward), z (vertical) directions. Θ and θ are mean and fluctuating virtual potential temperature (it will be called temperature hereafter), R and r are mean and fluctuating mixing ratio, f is the Coriolis parameter = -8.26×10^{-5} sec^{-1} at Hay, Australia (34°30'S, 144°56'E). Θ_o is a constant temperature and U_g and V_g are the geostrophic wind components introduced to replace the horizontal pressure gradient. In Eq. (3) the horizontal advection of Θ has been represented in terms of U_g and V_g utilizing the thermal wind relations.

To close the above set of equations, we need to express the turbulence second moments. We use the following equations in tensor form for turbulence variables:

$$\frac{\partial \overline{q^2}}{\partial t} = -2\left[\overline{uw}\frac{\partial U}{\partial z} + \overline{vw}\frac{\partial V}{\partial z}\right] - \frac{\partial}{\partial z}\left[\overline{q^2 w} + 2\overline{pw}\right] + 2g\beta\overline{w\theta} - 2\varepsilon \tag{5}$$

$$\frac{\partial \overline{\theta^2}}{\partial t} = -2\overline{w\theta}\frac{\partial \Theta}{\partial z} - \frac{\partial}{\partial z}\overline{w\theta^2} - 2\varepsilon_\theta \tag{6}$$

$$\frac{\partial \overline{\theta r}}{\partial t} = -\overline{wr}\frac{\partial \Theta}{\partial z} - \overline{w\theta}\frac{\partial R}{\partial z} - \frac{\partial \overline{w\theta r}}{\partial z} - 2\varepsilon_{\theta r} \tag{7}$$

$$\frac{\partial \overline{w\theta}}{\partial t} = -\overline{w^2}\frac{\partial \Theta}{\partial z} - \frac{\partial}{\partial z}(\overline{w^2\theta}) - \overline{\theta\frac{\partial p}{\partial z}} + g\beta\overline{\theta^2} \tag{8}$$

$$\frac{\partial \overline{wr}}{\partial t} = -\overline{w^2}\frac{\partial R}{\partial z} - \frac{\partial}{\partial z}(\overline{rw^2}) - \overline{r\frac{\partial p}{\partial z}} + g\beta\overline{\theta r} \tag{9}$$

$$\overline{u_j u_k}\frac{\partial U_i}{\partial x_j} + \overline{u_i u_j}\frac{\partial U_k}{\partial x_j} - \frac{2}{3}\overline{u_\ell u_j}\frac{\partial U_\ell}{\partial x_j}\delta_{ik} = \Pi_{ik} + [g_i\beta\overline{u_k\theta} + g_k\overline{u_i\theta} - \frac{2}{3}\delta_{ik}g\beta\overline{w\theta}] \tag{10}$$

for $i = 1,2,3$ and $k = j = 3$,

$$\overline{\theta u_j}\frac{\partial U_i}{\partial x_j} + \overline{u_i u_j}\frac{\partial \Theta}{\partial x_j} = -\Pi_i^\theta + g_i\beta\,\overline{\theta^2} \tag{11}$$

$$\overline{u_i u_j}\frac{\partial R}{\partial x_j} + \overline{u_j r}\frac{\partial U_i}{\partial x_j} = -\Pi_i^r + g_i\beta\,\overline{\theta r} \tag{12}$$

for $i = 1,2$ and $j = 3$

where $q^2 = u_i u_i$, $g_i = (0, 0, -1)g$, β is the coefficient of thermal expansion ($= \Theta_o^{-1}$), p is the pressure fluctuation divided by ρ_o , ε is the mean rate of turbulence energy dissipation, and ε_θ and $\varepsilon_{\theta r}$ are the mean rates of destruction of $\overline{\theta^2}/2$ and $\overline{\theta r}/2$ respectively. The pressure terms Π_{ik} , Π_i^θ and Π_i^r will be given shortly.

Eqs. (5) - (12) are very similar to those of MY except in the following two ways. According to MY's analysis of the order of magnitude, the diffusion terms in the equations for $\overline{u^2}$, $\overline{v^2}$ and $\overline{w^2}$ are small quantities. On the other hand, the observations indicate that these terms are quite important (Willis and Deardorff, 1974; Lenschow, 1970, 1974). Consequently, the diffusion terms are retained in our model. MY's analysis also indicates that the temporal variation terms for $\overline{w\theta}$ and $\overline{wr}$ are small quantities. We have retained

these terms in Eqs. (8) and (9) for convenience in numerically integrating the model. Otherwise the determination of $\overline{w\theta}$ and $\overline{wr}$ would require a complicated iterative solution to a set of simultaneous algebraic equations.

The pressure terms can be expressed as following (Launder, 1975; Zeman and Tennekes, 1975; ZL):

$$\Pi_{ik} = -\frac{1}{\tau} q^2 b_{ik} - \frac{3}{10} \beta (\overline{\theta u}_i g_k + \overline{\theta u}_k g_i - \frac{2}{3} \delta_{ik} \overline{\theta w})$$
$$+ \frac{2}{5} q^2 S_{ik} + q^2 \{ 2\alpha_1 (S_{ij} b_{jk} + S_{jk} b_{ij})$$
$$- \frac{2}{3} S_{j\ell} b_{\ell j} \delta_{ik}) + 2\gamma_1 (F_{ij} b_{jk} - F_{jk} b_{ij}) \} \qquad (13)$$

$$-\Pi_i^{\theta} = -\overline{\theta \frac{\partial p}{\partial x_i}}$$
$$= -\frac{c_\theta}{\tau} \overline{u_i \theta} + \frac{4}{5} \frac{\partial U_k}{\partial x_j} [\delta_{ik} \overline{u_j \theta} - \frac{1}{4} (\delta_{kj} \overline{u_i \theta} + \delta_{ji} \overline{u_k \theta})] - \frac{1}{3} g_i \beta \overline{\theta^2} \qquad (14)$$

$$-\Pi_i^{r} = -\overline{r \frac{\partial p}{\partial x_i}}$$
$$= -\frac{c_\theta}{\tau} \overline{u_i r} + \frac{4}{5} \frac{\partial U_k}{\partial x_j} [\delta_{ik} \overline{u_j r} - \frac{1}{4} (\delta_{kj} \overline{u_i r} + \delta_{ji} \overline{u_k r})] - \frac{1}{3} g_i \beta \overline{\theta r} \qquad (15)^*$$

where $S_{ik} = \frac{1}{2} (\frac{\partial U_i}{\partial x_k} + \frac{\partial U_k}{\partial x_i})$; $F_{ik} = \frac{1}{2} (\frac{\partial U_i}{\partial x_k} - \frac{\partial U_k}{\partial x_i})$;

$b_{ij} = (\overline{u_i u_j} - \frac{\delta_{ij}}{3} \overline{q^2}) / \overline{q^2}$, $\alpha_1 = \gamma_1 = 0.3$, $c_3 = 0.8$, $c_\theta = 2.17$,

$$\delta_{ij} = \begin{cases} 1 & \text{if } i = j \\ 0 & \text{otherwise} \end{cases}$$

and τ is the time scale defined as $\tau = \mu \overline{q^2} / \varepsilon$ with $\mu = 0.31$.

As we mentioned earlier, a simple gradient transport model of the type

$$\overline{q^2 u_i} \sim \tau \overline{u_i u_j} \frac{\partial \overline{q^2}}{\partial x_j}$$

is not adequate in a flow with buoyant effect. Hence we use the ZL model to calculate the diffusion terms, where

$$\overline{w\theta^2} = - K_t \frac{\partial \overline{\theta^2}}{\partial z} \tag{16}$$

$$\overline{w^2\theta} = -\{K_m \frac{\partial \overline{w\theta}}{\partial z} + 0.5\tau \overline{w\theta} \frac{\partial \overline{w^2}}{\partial z} - \frac{5}{6} g\beta\tau \overline{w\theta^2}\}/(1 + \frac{2\mu}{3}) \tag{17}$$

$$\overline{q^2 w + 2pw} = - \frac{3}{5}\{ K_m \frac{\partial \overline{w^2}}{\partial z} + 0.5\, K_m \frac{\partial \overline{q^2}}{\partial z} + \tau(\overline{uw} \frac{\partial \overline{uw}}{\partial z} + \overline{vw} \frac{\partial \overline{vw}}{\partial z}) \tag{18}$$

$$- \frac{3}{2} g\beta\tau \overline{w^2\theta}\}/(1 + \frac{5\mu}{3})$$

$$\overline{w\theta r} = - \{ (K_m + \frac{g\beta\tau\tau_\theta}{3\sigma} \overline{w\theta}) \frac{\partial \overline{\theta\gamma}}{\partial z} + \frac{g\beta\tau\tau_\theta}{6\sigma} (\overline{w\theta^2} \frac{\partial R}{\partial z} + \overline{wr} \frac{\partial \overline{\theta^2}}{\partial z})/ \tag{19}$$

$$(2 + \frac{g\beta\tau\tau_\theta}{3\sigma} \frac{\partial \Theta}{\partial z} + \frac{2\mu\tau}{\tau_\theta})$$

$$\overline{w^2 r} = - \{ K_m \frac{\partial \overline{w\theta}}{\partial z} + [\frac{\tau}{2} \overline{wr} \frac{\partial \overline{w^2}}{\partial z} - \frac{5}{6} g\beta\tau \overline{w\theta r}]\}/(1 + \frac{2\mu}{3}) \tag{20}$$

The eddy coefficients K_t and K_m are given by

$$K_t = \tau_c[\overline{w^2} + (b + \frac{1}{2\sigma}) g\beta\tau_\theta \overline{w\theta}]/(1 + \frac{\tau_c\tau_\theta}{2\sigma} g\beta \frac{\partial \Theta}{\partial z}) \tag{21}$$

$$K_m = \tau[\overline{w^2} + bg\beta\tau_\theta \overline{w\theta}] \tag{22}$$

where $\sigma = 1.0$, $b = 1.0$, $c_2 = 0.6$, τ_θ is the thermal time scale defined as $\tau_\theta = \mu\overline{\theta^2}/\varepsilon_\theta$ and the compound time scale τ_c is defined as

$$\tau_c = 1/[2.0/\tau + 2\mu/\tau_\theta]$$

The values of some parameters used above are slightly different from those in ZL. One reason for using slightly different values is that the approximations and equations used in this work are not exactly the same as ZL. Another reason is that a relatively large value of σ is required in order to produce a positive value of K_t near the ground surface (i.e., $\partial\Theta/\partial z < 0$) and in the inversion layer (i.e., where $\overline{w\theta} < 0$). We note that the values of the parameters used by Lumley et al. (1978) are not exactly the same as those used in ZL either, even though the formulations in these two papers are the same. According to Lumley et al. (1978), slight differences in the values of these parameters do not cause any significant difference in the result.

ZL proposed models of the dissipation equations in order to close the system. However, their models are quite complicated, involving many internal parameters. Since the small scale structure of turbulence at large Reynolds number is always approximately isotropic, we use the following simple MY model for dissipation:

$$\varepsilon = (2E)^{3/2}/\Lambda_1 \tag{23}$$

$$\varepsilon_\theta = (2E)^{1/2}\overline{\theta^2}/\Lambda_2 \tag{24}$$

$$\varepsilon_{\theta r} = (2E)^{1/2}\overline{\theta r}/\Lambda_2 \tag{25}$$

where $E = \overline{q^2}/2$ and Λ_1 , $\Lambda_2 = (15.0, 8.0)l$

The length scale l is given by

$$l = \begin{cases} l_u & \text{if } \frac{\partial\Theta}{\partial z} \le 0 \\ 1/[1.0/l_u + 1.0/l_s] & \text{if } \frac{\partial\Theta}{\partial z} > 0 \end{cases} \tag{26}$$

where

$$l_u = \frac{kz}{[1 + \frac{kz}{l_o}]} \quad , \quad l_s = \sqrt{2\ \overline{q^2}/(g\beta\frac{\partial\Theta}{\partial z})}$$

and $$l_o = \alpha S_\ell \frac{\int_o^\infty qz\,dz}{\int_o^\infty q\,dz}$$

In the above expression, $\alpha = 0.1$ and $S_\ell = \begin{cases} 0.75 + 1.25z/Z_I & \text{if } z < Z_I \\ 2.0 & \text{if } z \geq Z_I \end{cases}$

where Z_I is the depth of the mixed layer. Eq. (26) shows that the length scale of eddies near the ground is proportional to the height, whereas it is proportional to the penetration depth of a non-mixing parcel in the stable layer. A similar length scale in the stable layer has been used by Stull (1973) and Tennekes (1973). Note that the length scale obtained by Eq. (26) is continuous and smooth in the whole atmosphere. The set of equations (1) - (26) forms a closed system and will be solved numerically.

3. Initial and boundary conditions and numerical schemes

We use a vertically staggered grid with first and third moments calculated at the same main levels and second moments at the intermediate levels. The stretched vertical coordinate with a log-linear transformation is used (Sun and Ogura, 1979). The height of the first main level is at 4 m above the ground surface and the highest main level is at 2.05 km. There are 31 main levels in the vertical. A scheme with centered differencing in space and forward differencing in time is used (Sun and Ogura, 1979).

At the upper boundary, all turbulence variables and wind shear are set to zero, while the temperature and moisture are fixed during the computations. The heat and moisture fluxes at the ground surface are prescribed as functions of time, since the Wangara data do not include the surface temperature and moisture. The surface heat flux is assumed to take a sine law with a peak value of 21.6 K cm s^{-1} at 1300 EST and a half-period of 11 hours. The surface moisture flux has the same temporal form with a peak value of 2.29×10^{-5} cm s^{-1}. These values were derived by Wyngaard and Coté (1974) from the result of Deardorff's three-dimensional numerical simulation.

Following MY and WC, the roughness parameter, z_o, is set to 1 cm. The similarity equations proposed by Businger et al. (1971) are applied to the constant flux layer (a layer from the ground surface up to z = 4m in our model) to relate the most important turbulence variables, $\overline{uw}$, $\overline{vw}$, $\overline{w\theta}$ and $\overline{wr}$, to the mean variables U, V, Ⓗ and R. Other turbulence variables are calculated from MY's closure approximations.

The initial conditions at 0900 hours for Ⓗ, R and the time-independent geostrophic wind components U_g and V_g are exactly the same as those in Deardorff's numerical simulation. The initial conditions for the mean wind components U and V are the experimental data at 0900 hours which are smoothed to eliminate small

vertical oscillations. These initial conditions can be found from Figs. 1a, 3a, 5a and 6a. It is noted that U_g and V_g are time-independent variables in the model as they were in Deardorff's simulation.

The initial values of the second moments in the constant flux are calculated diagnostically as indicated earlier. Fig. 1a shows that the mixed layer was capped by the stable layer at an altitude Z_I = 130 m at 0900 hours. Consequently, all second moments except $\overline{q^2}$ at the initial time are assumed to decrease linearly with height in the mixed layer. All stresses and fluxes of heat and moisture are set to zero in the layer above the inversion, while small values (smaller than 10^{-3} times the values in the constant flux layer) are assigned to $\overline{\theta^2}$ and and $\overline{\theta r}$. The initial profile of $\overline{q^2}$ is such that $\overline{q^2}$ increases linearly in the lower portion of the mixed layer, takes a maximum value of about three times the $\overline{q^2}$ value in the constant flux layer at the midlevel in the mixed layer and then decreases gradually with height. Similar initial conditions were used by ZL and Sun and Ogura (1979). The third moments are calculated from Eqs. (16) through (22) after the first and second moments are determined.

The computer time required to compute one hour in physical time was 40 seconds for the present model on the CDC 7600 computer at the National Center for Atmospheric Research.

4. Results and discussions

a. Mean variables and turbulent fluxes

Figs. 1a and 1b show the time histories of the calculated and observed profiles of mean virtual potential temperature respectively. The overall agreement is satisfactory. Further, the expected shallow superdiabatic layer near the ground surface, the deep well-mixed layer and the inversion layer are well reproduced in the model. The calculated profiles are also in good agreement with numerical results obtained by Deardorff (1974a), Kuo and Sun (1976) and André et al. (1978). Recall that the radiative transfer is included in Deardorff's and André et al.'s models whereas it is not in our model. A comparison of these numerical results indicates that the radiative transfer does not contribute significantly to the temporal evolution of the temperature field during the daytime when the convective transport process dominates.

As indicated earlier, the surface fluxes of heat and moisture in our model are identical to those in WC. In this respect, it is of some interest to compare their result with ours. First, a physically unrealistic (although only slight) ground-based inversion develops after 1200 hours in their model, whereas it is absent in our result. Second, their temperature gradient changes gradually across the inversion layer so that the overshooting in the inversion layer is not as sharp as in our model. Third, their temperature in the mixed layer is about 0.2 to 0.3C higher than ours in the afternoon. This difference may be partly attributed to the horizontal advection cooling ($\simeq 0.012$ C hr^{-1}) which is included in our model and partly to the stronger downward heat flux in the inversion layer obtained by WC.

Fig. 2 shows the calculated vertical heat flux which linearly decreases with height in the mixed layer and becomes slightly negative near the inversion

layer. The downward heat flux at the inversion layer is between 4 to 7% of the upward surface heat flux. This is in good agreement with both the 5% observed by Lenschow in the atmosphere (1970, 1974) and the 5 to 8% obtained by Willis and Deardorff in their laboratory experiments (1974). Ratios in other references vary, including 14 to 21% in Deardorff's three-dimensional model (1974a); 5 to 12% in WC; less than 2% in Yamada and Mellor (1975), and 9 to 20% in ZL and Lumley et al. (1978). The ratio calculated by André et al. (1978) is about 15% in the afternoon. Zeman (1975) parameterized each term of the kinetic energy budget equation (5) in terms of the depth of the mixed layer, turbulence kinetic energy and the jumps of the [illegible]cal wi[illegible] across the inversion layer, with [illegible] ters which should be determined from experiments or [illegible] he atmosphe[illegible]. From this argument, Zeman concluded that th[illegible] eat flux at the inve[illegible] to that at the ground surface shou[illegible] nge from 0.05 to 0.[illegible] upper limit of 0.53 appears to be too [illegible] ch ob[illegible] in the atmosphere.

The calculated humidity profiles shown in Fig. 3a indicate that mixing ratio decreases (slightly but persistently) with height in the mixed layer. This result is consistent with the observations shown in Fig. 3b and the numerical result obtained by André et al. (1978). It is interesting to note that some other observations also show this slight decrease of humidity with height. They include Warner (1963), Warner and Telford (1967), Betts et al. (1974) and Wyngaard et al. (1978). The profiles in WC also decrease slightly with height. However, near the ground surface a spurious increase of humidity with height exists. In contrast, the humidity profiles in Deardorff's simulation do not show this tendency.

We noted that the Wangara data show a rather rapid decrease in humidity with time in the morning of Day 33 (Fig. 3b). None of the num[illegible]ical simulations to date, including ours, has been successful in predicting this rapid

decrease. It is suspected that this may be attributed to either an inaccurate estimate of the surface moisture flux employed in the models and/or the neglect of the horizontal moisture advection in the models.

The profiles of the moisture flux presented in Fig. 4 are very close to those obtained by André et al. (1978). The moisture supply from the ground surface is not as large as the moisture flux in the upper portion of the mixed layer. Consequently, the mixing ratio in the lower portion of the mixed layer decreases with time while the depth of the mixed layer increases (Fig. 3b).

A physically unrealistic downward moisture flux develops near the inversion in Deardorff's (1974a) and WC models, whereas it is not found in our model. An air parcel penetrating into the overlying stable layer is cooler and more moist than the surrounding air. The air moving downward to compensate such penetrating plumes is warmer and drier than the surrounding air in the inversion layer. Thus, the heat flux in the inversion layer should be downward whereas the moisture flux should be upward. This may also be related to the fact that the potential temperature is almost perfectly homogeneous in the mixed layer whereas the humidity decreases slightly with height, as indicated earlier.

The calculated x- and y- components of the mean wind are presented in Figs. 5a and 6a, respectively, along with the geostrophic wind components U_g and V_g. The observed mean wind profiles are shown in Figs. 5b and 6b. The overall agreement is good before 1500 hours. After that time the predicted wind is underestimated. The situation is similar to that shown by MY. The wind profiles obtained by André et al. (1978) are closer to the observations than are ours. This may be because André et al. adjusted U_g and V_g to correspond with the time variations found in the Wangara data whereas U_g and V_g were held constant in our model and in MY's.

The calculated profiles of turbulent fluxes of momentum are shown in Figs. 7 and 8. The vertical gradients of $\overline{u\,w}$ and $\overline{v\,w}$ are very large in the

inversion layer, corresponding to the sharp changes in U and V. André *et al.* (1978) noted using Eq. (1) that $\overline{uw}$ is a linear function of height in the mixed layer if V_g is small and towards the north as it is in the Wangara data. On the other hand, if U_g decreases linearly with height and U and V are well mixed, a differentiation of Eq. (2) with respect to z gives the parabolic profiles of $\overline{vw}$ in the mixed layer. These features are well reproduced in André *et al.* (1978) as well as in Figs. 7 and 8.

To facilitate a closer comparison with Deardorff's (1974a) result, Fig. 9 shows the wind profiles at 1500 hours obtained in Deardorff's model and in our model as well as the observed wind profiles in natural surface coordinates where the x axis is aligned with the wind direction in the surface layer. Fig. 10 shows a similar comparison, but for the surface wind direction. Apparently our result agrees with observations as well as or better than Deardorff's result. Since WC fixed the wind direction and the wind stresses at the ground surface during their experiment, no comparison with their result is made.

b. Eddy kinetic energy, other second moments and budgets

It is now well recognized that the scaling proposed by Deardorff (1970) can produce universal profiles of turbulence parameters in convective boundary layers. Following his argument, we use the following scaling factors in presenting our result: the depth of the mixed layer Z_I, the surface heat flux $\overline{w\theta}_s$, the surface moisture flux $\overline{wr}_s$, the convective velocity $w_* \ (= g\overline{w\theta}_s Z_I/\Theta_o)^{1/3}$, the convective temperature $\theta_* \ (= \overline{w\theta}_s/w_*)$ and the convective humidity $r_* \ (= \overline{wr}_s/w_*)$. Table 1 gives the values of these scaling factors used in our model.

The calculated dimensionless vertical velocity variance, σ_w^2/w_*^2 , is presented in Fig. 11. The model results are in excellent agreement with the Minnesota data in the lower mixed layer (i.e., $z < 0.5\ Z_I$), whereas they fall slightly lower than the atmospheric data in the upper mixed layer (i.e., $z > 0.5\ Z_I$). It is also interesting to note that, according to Caughey and Palmer (1979), σ_w^2 does not vanish even at $z = 1.4\ Z_I$. They indicated that the finite value of σ_w^2 above Z_I is associated with entrainment and, at the higher levels particularly, with internal waves. These show up clearly in the temperature contours and have periods in the range 5-10 minutes (Palmer et al., 1979). These internal waves are also indicated in the numerical simulation of Kuo and Sun (1976).

Fig. 12 shows the average of the horizontal velocity variances, $\sigma_{u,v}^2$, normalized by w_*^2 . Caughey and Palmer (1979) indicated that the Minnesota and Ashchurch data are in excellent agreement with the aircraft data (summarized by Willis and Deardorff). The data from Willis and Deardroff's laboratory experiment falls substantially lower than the atmospheric data but have the same general shape. The results from our model are much smaller in magnitude than those from the laboratory experiments and the atmospheric observations. The model results become worse as the ground surface is approached. We may attribute the deficiency of our model to the following.

This study follows Mellor and Yamada's formulation and assumes the following form of the similarity theory for the standard deviations for turbulent velocity components in the surface layer:

$$\frac{\sigma_\alpha}{u_*} = \phi_\alpha\left(\frac{z}{L}\right) , \qquad \alpha = u , v , w \tag{4.1}$$

where u_* is the surface friction velocity and L the Monin-Obukhov length. ϕ is presumed to represent a set of universal functions. Lumley and Panofsky

(1964) noted that Eq. (4.1) applies well to vertical but not to horizontal velocity components. Subsequently, Wyngaard and Coté (1974) and Panofsky et al. (1977) proposed that the standard deviations of horizontal velocity components under convective conditions are described by

$$\frac{\sigma_\alpha}{u_*} = \phi_\alpha\left(\frac{Z_I}{L}\right) , \qquad \alpha = u , v \tag{4.2}$$

Panofsky et al. also showed that Eq. (4.2) fits the observation data well. A possible improvement of our model with inclusion of Eq. (4.2) is left for future work.

Fig. 13 shows the eddy kinetic energy budget at 1400 hours. The result is quite similar to that calculated by André et al. (1978). The dissipation rate ε and buoyant production $B = g\beta\overline{w\theta}$ are the dominant terms in the eddy kinetic energy budget equation and these two effects nearly cancel out each other. The transport term $T = -(\overline{q^2 w}/2 + \overline{pw})/\partial z$ is also important because turbulence in the inversion layer is sustained by this process against the disspation and the negative buoyant production. The wind shear production $M = -(\overline{uw}\partial U/\partial z + \overline{vw}\partial V/\partial z)$ is negligibly small in the entire mixed layer, except near the ground surface and in the inversion layer.

The calculated dimensionless temperature variance $\overline{\theta^2}/\theta_*^2$ is shown in Fig. 14. It decreases rapidly with height in the lower and mid-regions of the mixed layer. There is a local maximum near the top of the mixed layer. The numerical results relate quite well in shape and magnitude to the Minnesota data in the lower and mid-regions of the mixed layer. They approach to a local minimum near $z = 0.8\ Z_I$, and then increase again to form a local maximum at the top of the mixed layer. The short dashed line in Fig. 14 represents the free convection prediction (Kaimal et al., 1976) and is given by

$$\overline{\theta^2}/\theta_*^2 = 1.8(z/Z_I)^{-2/3} \tag{4.3}$$

This line is seen to provide a fairly good fit to the observational data and to our results up to 0.2 Z_I. On the other hand, Willis and Deardorff's data fall lower than the atmospheric data in mid-region of the mixed layer. Further, the temperature variance at the top of the convective boundary layer from our study appears to be substantially lower than those from the laboratory experiments or from the atmospheric observations. It is also underestimated above the inversion layer. The temperature variance near and above the inversion base is associated with the entrainment and internal gravity waves (Kuo and Sun, 1976; Caughey and Palmer, 1979). Therefore, the dissipation rate near the inversion layer can be significantly different from that in the convective boundary layer. This process is not incorporated into our model.

The virtual potential temperature variance budget presented in Fig. 15 is somewhat different from those obtained by Deardorff (1974b) and André et al. (1978). The results in these two earlier works are also somewhat different from each other. The production term $M = -\overline{w\theta}\,\partial\Theta/\partial Z$ shown in Fig. 15 is larger than those calculated by Deardorff or André et al. Lenschow's aircraft measurement (1970) indicates negative M in the main body of the mixed layer, because the atmosphere at the time of his observations was slightly stably stratified. The diffusion $T = -0.5\,\partial\overline{w\theta^2}/\partial z$ in the lower portion of the mixed layer shown in Fig. 15 is smaller than those obtained from the aircraft measurement or obtained by André et al. The diffusion obtained by Deardorff and ZI becomes negative in the lower portion of the mixed layer. This does not agree with the aircraft measurements by Telford and Warner (1964), Lenschow (1970), or the laboratory measurement by Ferriera (1978). The dissipation ε_θ in the mixed layer shown in Fig. 15 agrees with the observation or the result of André et al. In the inversion layer, the magnitudes of M and ε_θ shown in Fig. 15 are consistent with Lenschow's aircraft measurements, whereas those calculated by Deardorff and André et al. appear to be considerably overestimated when compared to aircraft observations.

Fig. 16 shows the calculated profile of temperature-humidity covariance at 1400 hours, which evidently agrees very well with the aircraft measurement by Wyngaard et al. (1978) on a dimensionless scale. A strong negative correlation exists between the fluctuating temperature and humidity in the inversion layer in contrast to a strong position correlation existing near the ground surface. This behavior is easily understood; the air penetrating into the overlying stable layer is cooler and more moist than the surrounding air. On the other hand, the rising parcel is warmer and more moist than the surrounding air in the lower mixed layer.

The calculated profiles of the rate of kinetic energy dissipation (ε), the fundamental length scale (ℓ) and the time scale (τ) at 1400 hours are presented in Fig. 17. Similar profiles of ε are calculated by Deardorff (1974b) and ZL, but with a slightly smaller magnitude. On the other hand, Yamada and Mellor's result does not show a sharp decrease with height in the inversion layer, even though their formulation for ε is almost identical to ours. Also ℓ in Fig. 17 is very small compared to Yamada-Mellor's ℓ near the top of the mixed layer. This is because ℓ in our model is proportional to the penetration depth of a non-mixing air parcel into the stable layer (Stull, 1973) and $\overline{q^2}$ is very small in the inversion layer. It is also noted that the shape of ℓ in Fig. 17 is similar to that for the peak wavelength in the vertical velocity spectra estimated from the Minnesota and Ashchurch experiments (Caughey and Palmer, 1979).

c. Third moments

Fig. 18 compares the calculated profile of the dimensionless turbulent kinetic energy flux with ZL and the observations. Our result is quite close to that calculated by André et al. It agrees well with the observations in the upper portions of the mixed layer. However, it is only 50 to 70% of the observational values in magnitudes in the middle and lower portions of the mixed layer. On the other hand, ZL's result is in good agreement with the observation in the lower portion of the mixed layer whereas it overestimates in the middle and upper portions.

The calculated profiles of $\overline{w^2\theta}$ at 1400 hours is shown in Fig. 19, along with the results from field observations, a laboratory experiment and the model of ZL. We observed that our result lies between ZL's and experimental results in the upper portion of the mixed layer. However ZL's result agrees with the experimental result better than ours in the lower portion of the mixed layer. The observational results scatter rather widely. Thus it is rather difficult to evaluate which model produces the better result. We also note that the term $-\overline{w'^3}(\partial \Theta / \partial Z)$ was ignored in ZL's (as well as ours) transport model in calculating $\overline{w^2\theta}$. This ignored term may significantly affect the result of $\overline{w^2\theta}$ in the lower portion of the mixed layer where $-\partial \Theta / \partial Z$ is large and may bring the model predicted $\overline{w^2\theta}$ closer to the measured values (Ferriera, 1978). This assessment has not been done in this work, however.

Fig. 20 shows that the predicted $\overline{\theta^2 w}$ agrees well with the field observations in the entire mixed layer. However, the experimental results from Ferreira (1978) are much larger than the field observations. The results of ZL are slightly larger than ours for $z > 0.1\ Z_I$. However, $\overline{\theta^2 w}$ predicted by ZL decreases in magnitude with decreasing z in the layer below $0.1\ Z_I$. This behavior does not agree with observational or experimental results shown in Fig. 20.

Finally Fig. 21 presents the calculated profiles of $\overline{w^2 r}$ and its vertical derivative at 1400 hours. The parameter $-\partial \overline{w^2 r}/\partial z$ is negative in the mixed layer and positive in the inversion layer, corresponding to the processes whereby moisture in the mixed layer is pumped into the inversion layer by convective turbulence. Further, $-\partial \overline{w^2 r}/\partial z$ is of the same order of magnitude as $g\beta\overline{\theta r}$ in Eq. (9) in the inversion layer. Thus, the result indicates that the third-order flux terms, $\partial \overline{w^2\theta}/\partial z$ and $\partial \overline{w^2 r}/\partial z$, should be retained in the equations for the vertical heat and moisture fluxes.

5. Summary

A model for a moist planetary boundary layer is developed based on the general framework of the Level 3 turbulence closure model proposed by Mellor and Yamada (1974). The model includes five prognostic equations; one each for the total turbulent kinetic energy, virtual potential temperature variance, covariance between temperature and humidity, vertical heat flux and vertical moisture flux. All other turbulence variables are determined diagnostically from algebraic equations. The third moments and the pressure terms involved in these equations are calculated using the formulations of Zeman and Lumley (1976). Further, a length scale in a stable layer is introduced in the model.

The model is applied to Day 33 daytime of the Wangara data. The result is compared not only to the Wangara data, but also to other observational and experimental data from various sources, to the result from Deardorff's three-dimensional simulation of the planetary boundary layer as well as to the results from the more complex second-order model by Zeman and Lumley (1976) and the third-order model by André et al. (1978). It is found that the mean wind, virtual potential temperature and moisture profiles observed in the Wangara experiment are well simulated by the present model. Further, the model result for the second and third moments is in good agreement with the aircraft measurements and laboratory experiments. The agreement is as good as, or somewhat better in some aspects (including predictions of mean wind, mean moisture and moisture flux) than obtained by Wyngaard and Coté (1974) and Deardorff (1974a,b).

Our result indicates that the third moments are not negligibly small, contrary to Yamada and Mellor's (1975) postulation. Further, the vertical profile of the rate of turbulence kinetic energy dissipation ε is found to be closer to that of Zeman and Lumley or

Deardorff than to that of Yamada and Mellor, even though the formulation of ε in the model is identical with that in Yamada and Mellor. This may indicate that the diffusion terms are not adequately represented in Yamada and Mellor. The result also supports Deardorff's proposal (1970) that universal profiles of turbulence variables can be produced in the convective planetary boundary layer when these variables are properly scaled.

Despite these favorable comparisons with the observational and experimental results, the present model includes some deficiencies. The model underpredicts the horizontal turbulence variances $\overline{u^2}$ and $\overline{v^2}$. The similarity law proposed by Wyngaard and Coté (1974) and Panofsky et al. (1977) may circumvent this deficiency. Furthermore, Lumley (1978) challenges the concept of quasi-Gaussianity which is a standard assumption in the ZL transport model. More efforts should be exerted to improve the model.

In a recent article, the authors (1979) applied Mellor and Yamada's Level 3 model to a two-dimensional simulation of the boundary layer processes associated with the formation of a squall line along the dry line over Oklahoma. The model simulated well the overall behavior of the planetary boundary layer and the formation of the prestorm low-level convergence which subsequently triggered the development of the squall line (Ogura and Chen, 1977). However, the turbulence momentum transport across the inversion layer appeared to be underestimated. This process of transfer of the westerly momentum from high to low levels is presumably important in generating low-level convergence. The work presented in this article is a step in our development of a planetary boundary layer parameterization which hopefully will be accurate and simple enough to be incorporated into two- or three-dimensional meso- or synoptic-scale prediction models.

Acknowledgements

The authors wish to thank Drs. F. B. Lipps, G. L. Mellor, I. Orlanski, and R. Wilhelmson who read the draft of this paper and offered many useful comments and constructive criticisms to improve the paper. Dr. J. E. Wyngaard also offered many valuable comments. K. Garrelts and D. McNeely typed the manuscript and J. Brother drafted the figures. The work was supported by the National Science Foundation under Grant No. ATM78-01010 and the Environmental Research Laboratories, National Oceanic and Atmospheric Administration under Grant No. 04-7-002-44026. The main part of the numerical computation was done at the National Center for Atmospheric Research which is supported by the National Science Foundation. The Research Board of the University of Illinois also provided computer support.

Table 1. Scaling parameters for Day 33 of the Wangara experiment calculated from the model

Time (hr)	Z_I(m)	w_* (cm/s)	θ_*(K)	r_*
1000	219	1.03×10^{2}	1.39×10^{-1}	1.48×10^{-5}
1200	881	1.86×10^{2}	1.13×10^{-1}	1.19×10^{-5}
1400	1095	1.99×10^{2}	1.04×10^{-1}	1.10×10^{-5}
1600	1210	1.81×10^{2}	7.81×10^{-2}	8.28×10^{-6}

REFERENCES

André, J. C., G. De Moor, P. Lacarrère, and R. du Vachat, 1976a: Turbulence approximation for inhomogeneous flow: Part I. The clipping approximation. J. Atmos. Sci., 33, 476-481.

_____, _____, _____, and _____, 1976b: Turbulence approximation for inhomogeneous flows. Part II: The numerical simulation of a penetrative convection experiment. J. Atmos. Sci., 33, 482-491.

_____, _____, _____, G. Therry, and R. du Vachat, 1978: Modeling the 24-hour evolution of the mean and turbulent structures of the planetary boundary layer. J. Atmos. Sci., 35, 1861-1883.

Betts, A. K., F. J. Dugan and R. W. Grover, 1974: Residual errors of the VIZ radiosonde hygristor as deduced from observations of sub-cloud layer structure. Bulletin, Amer. Meteor. Soc., 55, 1123-1125.

Businger, J. A., J. C. Wyngaard, Y. Isumi, and E. F. Bradley, 1971: Flux-profile relationships in the atmosphere surface layer. J. Atmos. Sci., 28, 181-189.

Caughey, S. J., and S. G. Palmer, 1979: Some aspects of turbulence structure through the depth of the convective boundary layer. Quart. J. Roy. Meteor. Soc., 105, 811-827.

Chung, M. K., 1978: Study of second order turbulence models with variable coefficients. Ph.D. thesis, University of Illinois.

Deardorff, J. W., 1970: Convective velocity and temperature scales for the unstable planetary boundary layer and for Rayleigh convection. J. Atmos. Sci., 27, 1211-1213.

_____, 1974a: Three-dimensional numerical study of the height and mean structure of a heated planetary boundary layer. Boundary-Layer Meteor., 7, 81-106.

_____, 1974b: Three-dimensional numerical study of turbulence in an entraining mixing layer. Boundary-Layer Meteor., 7, 199-226.

Ferreira, R., 1978: Unsteady turbulent thermal convection. Ph.D. thesis, University of Illinois.

Hanjalic, K., and D. E. Launder, 1972: Fully developed asymmetric flow in a plane channel. J. Fluid Mech., 52, 609-638.

Kaimal, J. C., J. C. Wyngaard, D. A. Haugen, O. R. Coté, Y. Izumi, S. J. Caughey, and C. J. Readings, 1976: Turbulence structure in the convective boundary layer. J. Atmos. Sci., 33, 2152-2169.

Kuo, H. L., and W. Y. Sun, 1976: Convection in the lower atmosphere and its effects. J. Atmos. Sci., 33, 21-40.

Launder, B. E., 1975: On the effects of a gravitational field on the turbulent transport of heat and momentum. J. Fluid Mech., 67, 569-581.

Lenschow, D. W., 1970: Airplane measurements of planetary boundary layer structure. J. Appl. Meteor., 9, 874-884.

_____, 1974: Model of the height variation of the turbulent kinetic energy budget in the unstable planetary boundary layer. J. Atmos. Sci., 31, 465-474.

REFERENCES (cont')

_____, and W. B. Johnson, Jr., 1968: Concurrent airplane and balloon measurements of atmospheric boundary-layer structure over a forest. J. Appl. Meteor., 7, 79-89.

Lumley, J. L., 1978: Computational modeling of turbulent flows. Adv. Appl. Mech., 18, 123-176.

_____, and B. Khajeh-Nouri, 1974: Computational modeling of turbulence transport. Adv. in Geophys., A 18, 169-192.

_____, and H. A. Panofsky, 1964: Structure of Atmospheric Turbulence. Wiley-Interscience, New York.

_____, O. Zeman and J. Siess, 1978: The influence of buoyancy on turbulent transport. J. Fluid Mech., 84, 581-597.

Mellor, G. L., and T. Yamada, 1974: A hierarchy of turbulence closure models for planetary boundary layers. J. Atmos. Sci., 31, 1791-1806.

Ogura, Y., and Y. L. Chen, 1977: A life history of an intense mesoscale convective storm in Oklahoma. J. Atmos. Sci., 33, 1458-1476.

Palmer, S. G., S. J. Caughey, and K. W. Whyte, 1979: An observational study of entraining convection using balloon-borne turbulence probes and high power doppler radar. Boundary-Layer Meteor., 16, 261-278.

Panosky, H. A., H. Tennekes, D. H. Lenschow, and J. C. Wyngaard, 1977: The characteristics of turbulent velocity components in the surface layer under convective conditions. Boundary-Layer Meteor., 11, 355-361.

Pielke, R. A., and Y. Mahrer, 1975: Representation of the heated planetary boundary layer in Mesoscale Models with Coarse Vertical Resolution. J. Atmos. Sci., 32, 2288-2308.

Stull, R. B., 1973: Inversion-rise model based on penetrative convection. J. Atmos. Sci., 30, 1092-1099.

Sun, W.-Y., and Y. Ogura, 1979: Boundary layer forcing as a possible trigger to a squall line formation. J. Atmos. Sci., 36 (in print).

Telford, J. W., and J. Warner, 1964: Fluxes of heat and vapor in the lower atmosphere derived from aircraft observations. J. Atmos. Sci., 21, 539-548.

Tennekes, H., 1973: A model for the dynamics of the inversion above a convective boundary layer. J. Atmos. Sci., 30, 558-567.

Warner, J., 1963: Observations relating to theoretical models of a thermols. J. Atmos. Sci., 20, 546-550.

_____, and J. W. Telford, 1967: Convection below cloud base. J. Atmos. Sci., 24, 374-382.

Willis, G. E., and J. W. Deardorff, 1974: A laboratory model of the unstable planetary boundary layer. J. Atmos. Sci., 31, 1297-1307.

REFERENCES (cont')

Wyngaard, J. E., and O. R. Cote, 1974: The evolution of the convective planetary boundary layer - A higher-order closure model study. Boundary-Layer Meteor., 7, 289-308.

_____, W. T. Pennell, D. H. Lenschow and M. A. LeMone, 1978: The temperature-humidity covariance budget in the convective boundary layer. J. Atmos. Sci., 35, 47-58.

Yamada, T., and G. L. Mellor, 1975: A simulation of the Wangara atmospheric boundary layer data. J. Atmos. Sci., 32, 2309-2329.

Zeman, O., 1975: The dynamics of entrainment in the planetary boundary layer: a study in turbulence modeling and parameterization. Ph.D. thesis, The Pennsylvania State University.

_____, and J. L. Lumley, 1976: Modeling buoyancy driven mixed layers. J. Atmos. Sci., 33, 1974-1988.

_____, and H. Tennekes, 1975: A self-contained model for the pressure terms in turbulent stress equations of the neutral atmospheric boundary layer. J. Atmos. Sci., 32, 1808-1813.

Figure legends

Fig. 1a. Calculated profiles of mean virtual potential temperature during Day 33 of the Wangara experiment.

Fig. 1b. Observed profiles of mean virtual potential temperature.

Fig. 2. Calculated profiles of the vertical heat flux.

Fig. 3a. Calculated profiles of mean mixing ratio.

Fig. 3b. Observed profiles of mean mixing ratio.

Fig. 4. Calculated profiles of the vertical moisture flux.

Fig. 5a. Calculated profiles of the x-component of the mean wind.

Fig. 5b. Observed profiles of the x-component of the mean wind.

Fig. 6a. Calculated profiles of the y-component of the mean wind.

Fig. 6b. Observed profiles of the y-component of the mean wind.

Fig. 7. Calculated profiles of the x-component of momentum flux.

Fig. 8. Calculated profiles of the y-component of momentum flux.

Fig. 9. Wind profiles at 1500 hours observed (denoted by open circles and closed circles), calculated by Deardorff (1974a) (denoted by U_D and V_D) and calculated from the present model (denoted by U and V) in natural surface-layer coordinates. The geostrophic wind components (U_g and V_g) are also included.

Fig. 10. Surface wind direction (degrees from north). Direction calculated by Deardorff (1974a) is denoted by bold solid curve, direction from the present model is denoted by dashed curve, observed direction by thin solid curve, observed geostrophic flow direction by dash-dotted curve; assumed geostrophic flow direction is from 90°.

Fig. 11. Vertical velocity variance, σ_w^2, normalized by w_*^2. The solid line is the model prediction at 1400 hours; the dash-dot line indicates the average of the S1 and S2 cases in Willis and Deardorff (1974); the dashed line is the free convection prediction, $\sigma_w^2/w_*^2 = 1.8(z/z_I)^{2/3}$ in Kaimal et al. (1976). The Minnesota and Ashchurch data are shown by open and closed circles respectively.

Fig. 12. The average of the horizontal velocity variances, $\sigma^2_{u,v}$, normalized by w_*^2. The solid line is the model prediction at 1400 hours; the dashed line indicates Deardorff's numerical results; large closed circles and triangles represent Willis and Deardorff's results. The Minnesota and Ashchurch data are coded as in Fig. 11.

Fig. 13. Eddy kinetic energy budget at 1400 hours; B, buoyant production; M, mechanical (shear) production; $-\varepsilon$, dissipation; T, turbulent transport. The variables are made dimensionless by w_*^3/z_I ($= 71.8\ cm^2\ sec^{-3}$).

Fig. 14. The normalized temperature variance at various times. The short dashed line represents the free convection prediction, $\overline{\theta}^2/\theta_*^2 = 1.8(z/z_I)^{-2/3}$. Closed circles indicate Willis and Deardorff's results and open circles the Minnesota data.

Fig. 15. Virtual potential temperature variance budget at 1400 hours: M, mechanical production; $-\varepsilon_\theta$, molecular destruction; T, turbulent transport. The variables are made dimensionless by $w_*\theta_*^2/z_I$ ($= 1.96 \times 10^{-5}\ K^2\ sec^{-1}$).

Fig. 16. Calculated profile of temperature-humidity covariance at 1400 hours. The aircraft measurements by Wyngaard et al. (1978) are also included.

Fig. 17. Calculated profiles of the rate of kinetic energy dissipation (ε), the length scale (ℓ) and the time scale (τ) at 1400 hours.

Fig. 18. Calculated profile of dimensionless turbulent energy flux (solid line) at 1400 hours compared with Zeman and Lumley (1976, dash-dotted line) and observed data: solid circles and triangles, Willis and Deardorff (1974); open circles and triangles, Lenschow (1970, 1974) and Lenschow and Johnson (1968).

Fig. 19. Calculated profile of $\overline{w^2\theta}$ at 1400 hours.

Fig. 20. Calculated profile of $\overline{w\theta^2}$ at 1400 hours.

Fig. 21. Calculated profiles of $\overline{w^2 r}$ (solid line) and $-\partial\overline{w^2 r}/\partial z$ (dashed line) at 1400 hours.

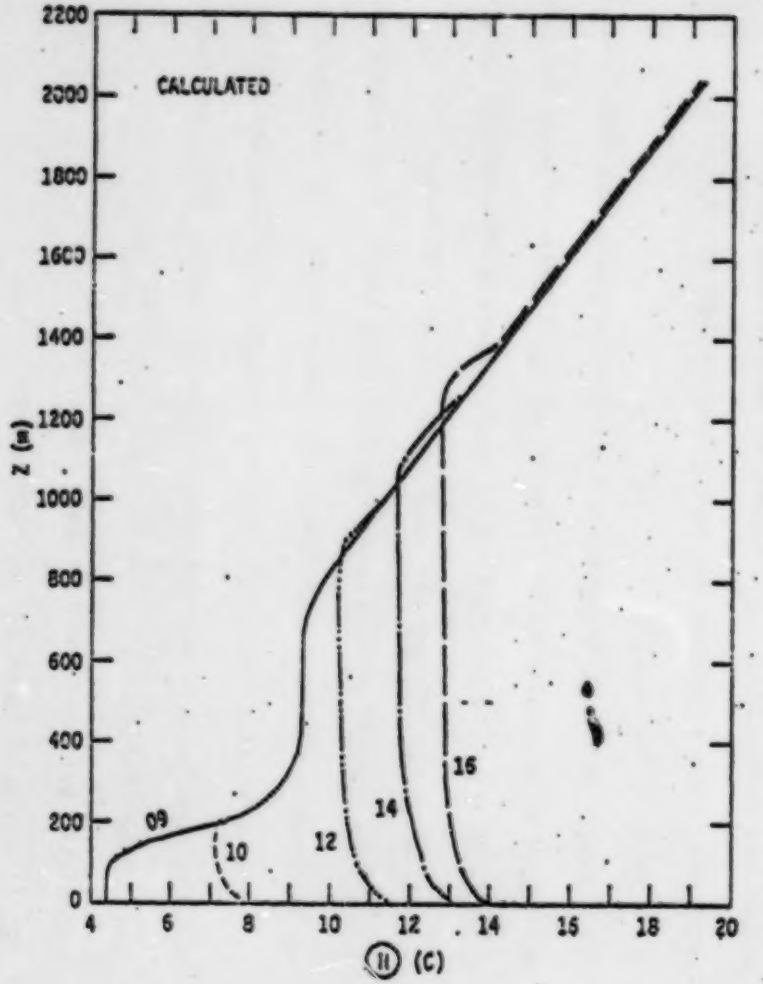
CALCULATED
Z (m)
2200
2000
1800
1600
1400
1200
1000
800
600
400
200
0
09
10
12
14
16
4
6
8
10
12
14
16
18
20
(H) (C)

Fig. 1a

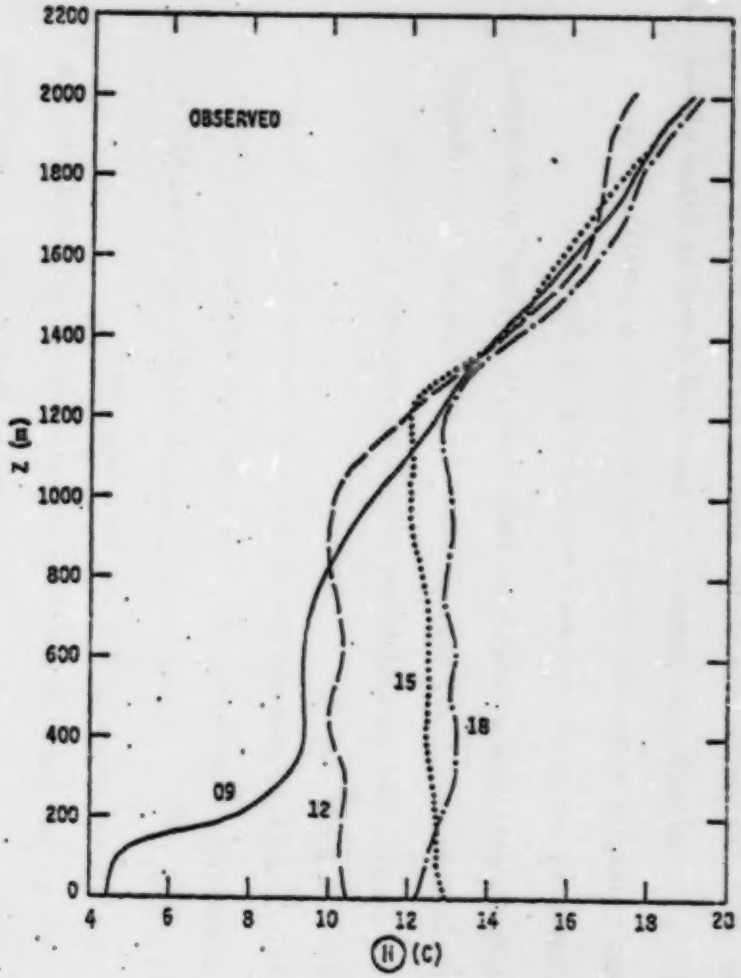
OBSERVED
Z (m)
2200
2000
1800
1600
1400
1200
1000
800
600
400
200
0
09
12
15
18
4
6
8
10
12
14
16
18
20
(H) (C)

Fig. 1b

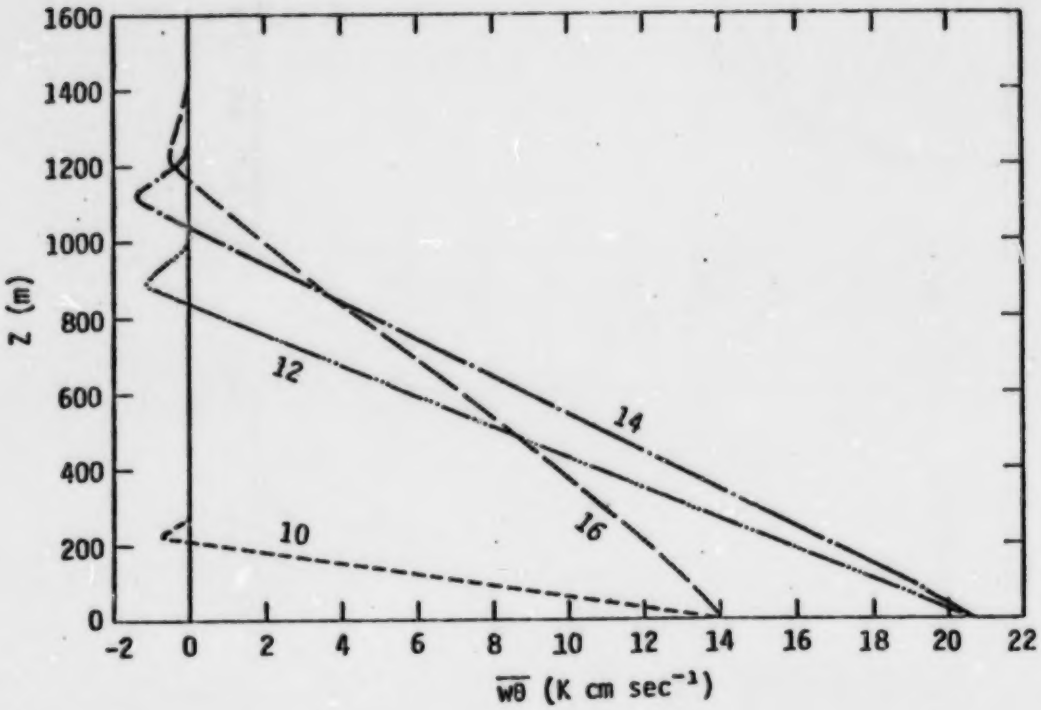
1600
1400
1200
1000
800
600
400
200
0
z (m)
-2
0
2
4
6
8
10
12
14
16
18
20
22
$\overline{w\theta}$ (K cm sec^{-1})
12
14
16
10

Fig. 2

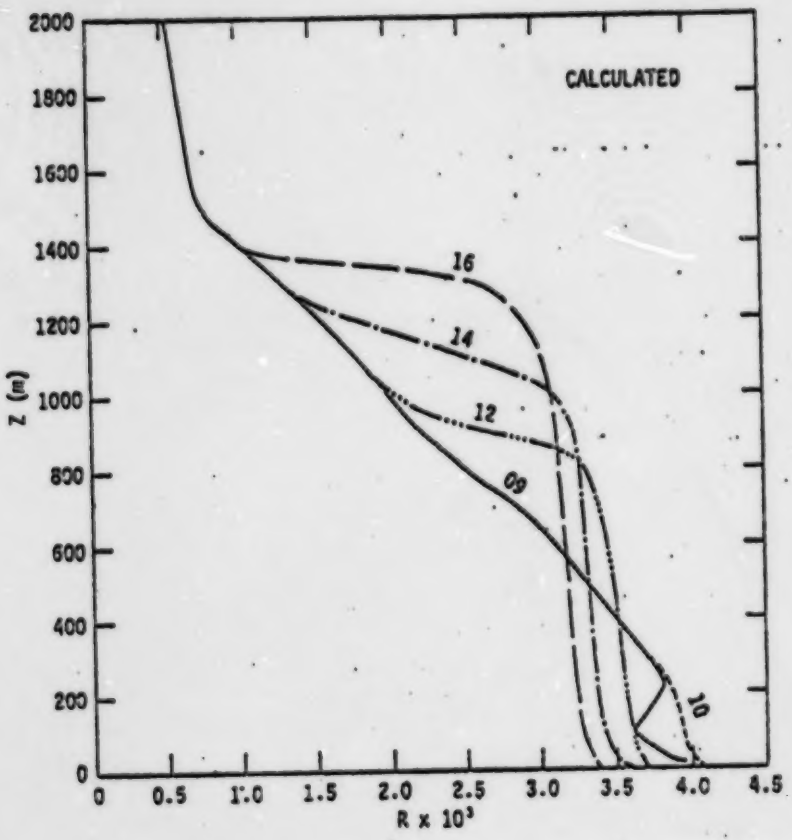
CALCULATED
16
14
12
09
10
z (m)
R x 10³
0
200
400
600
800
1000
1200
1400
1600
1800
2000
0.5
1.0
1.5
2.0
2.5
3.0
3.5
4.0
4.5

Fig. 3a

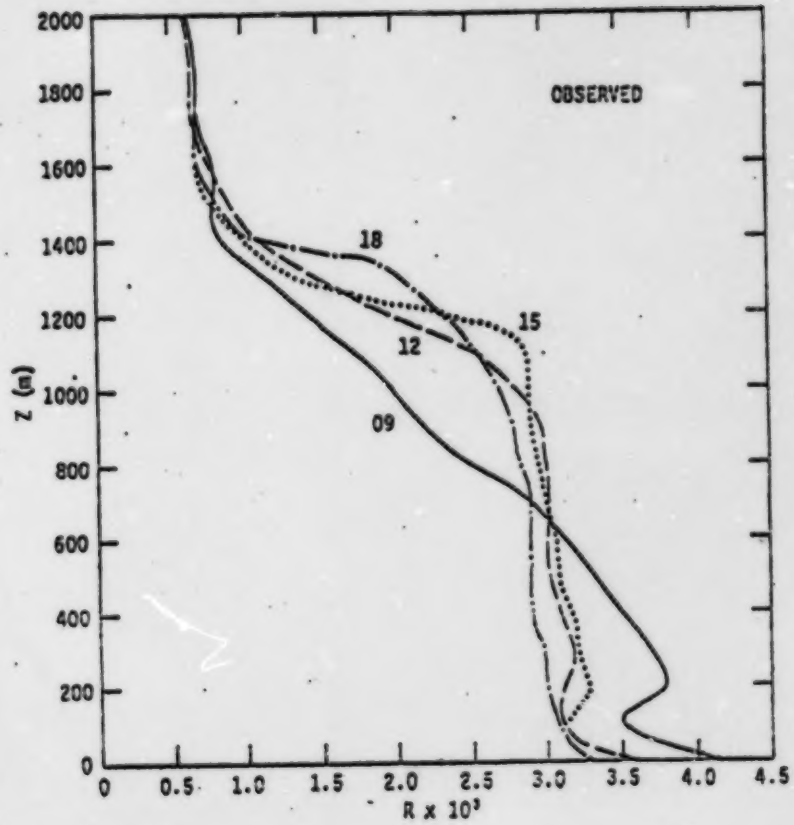
OBSERVED
18
15
12
09
z (m)
R x 10³
0
200
400
600
800
1000
1200
1400
1600
1800
2000
0.5
1.0
1.5
2.0
2.5
3.0
3.5
4.0
4.5

Fig. 3b

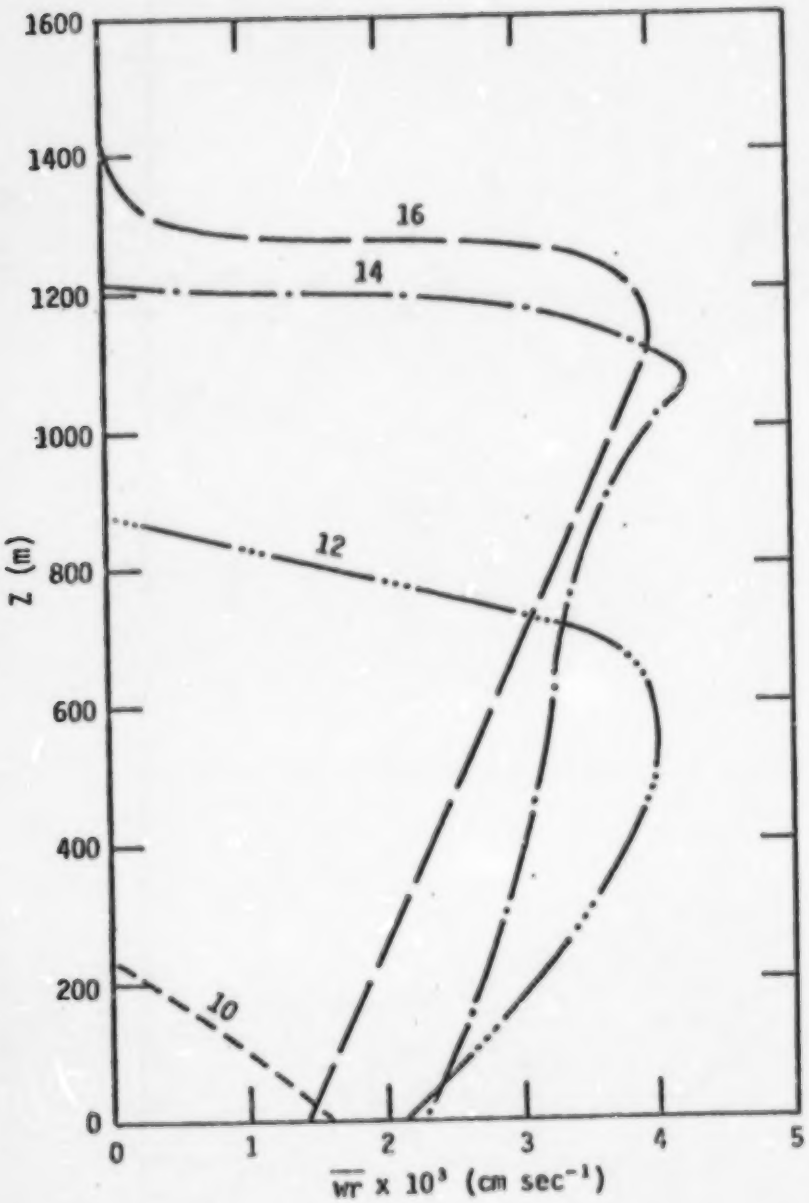
1600
1400
1200
1000
800
600
400
200
0
Z (m)
16
14
12
10
0
1
2
3
4
5
$\overline{wr}$ x 10^3 (cm sec^{-1})

Fig. 4

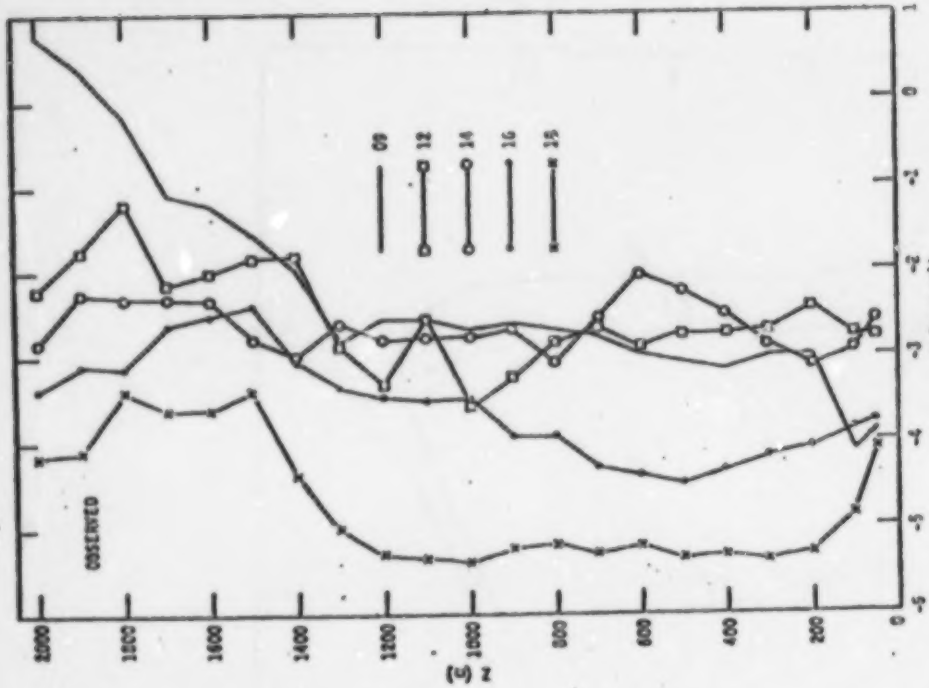

Fig. 5b

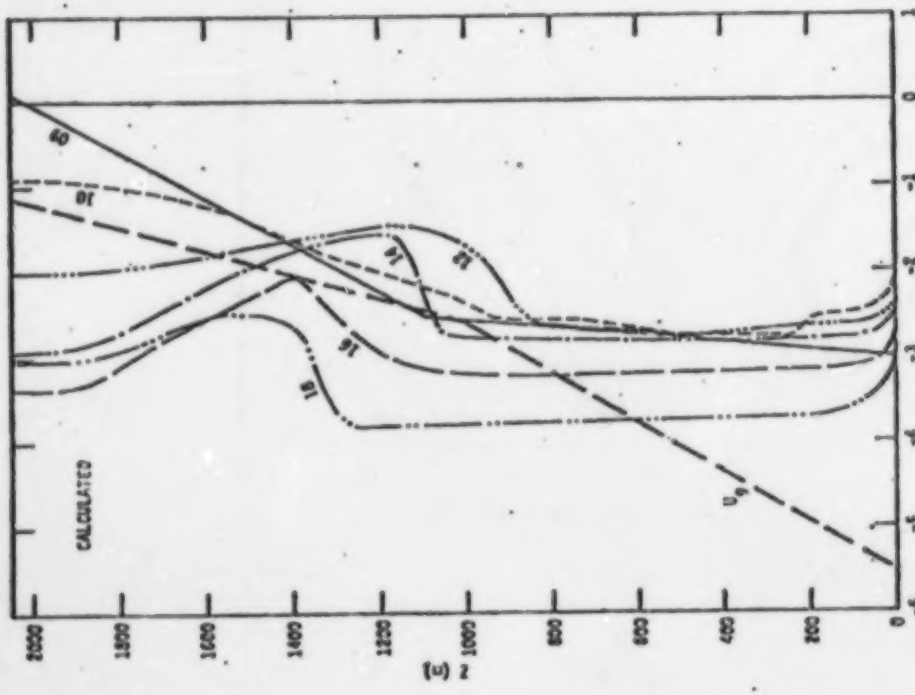

Fig. 5a

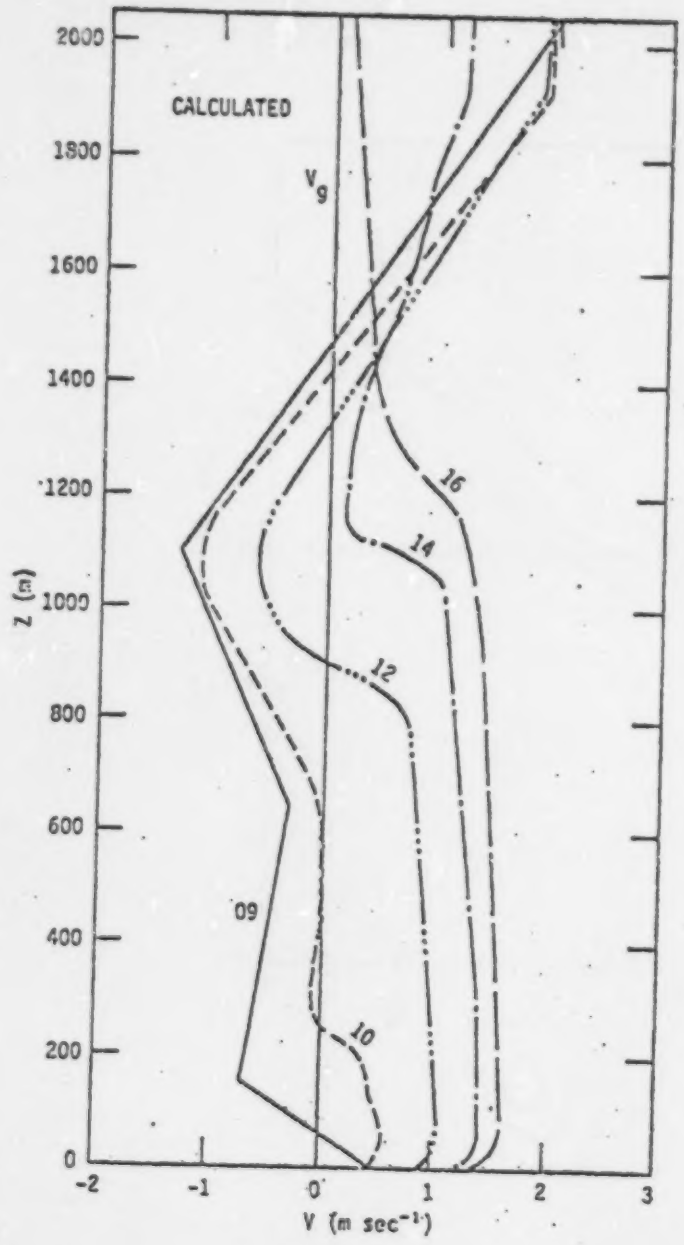
CALCULATED
V_g
16
14
12
09
10
Z (m)
V (m sec^{-1})

Fig. 6a

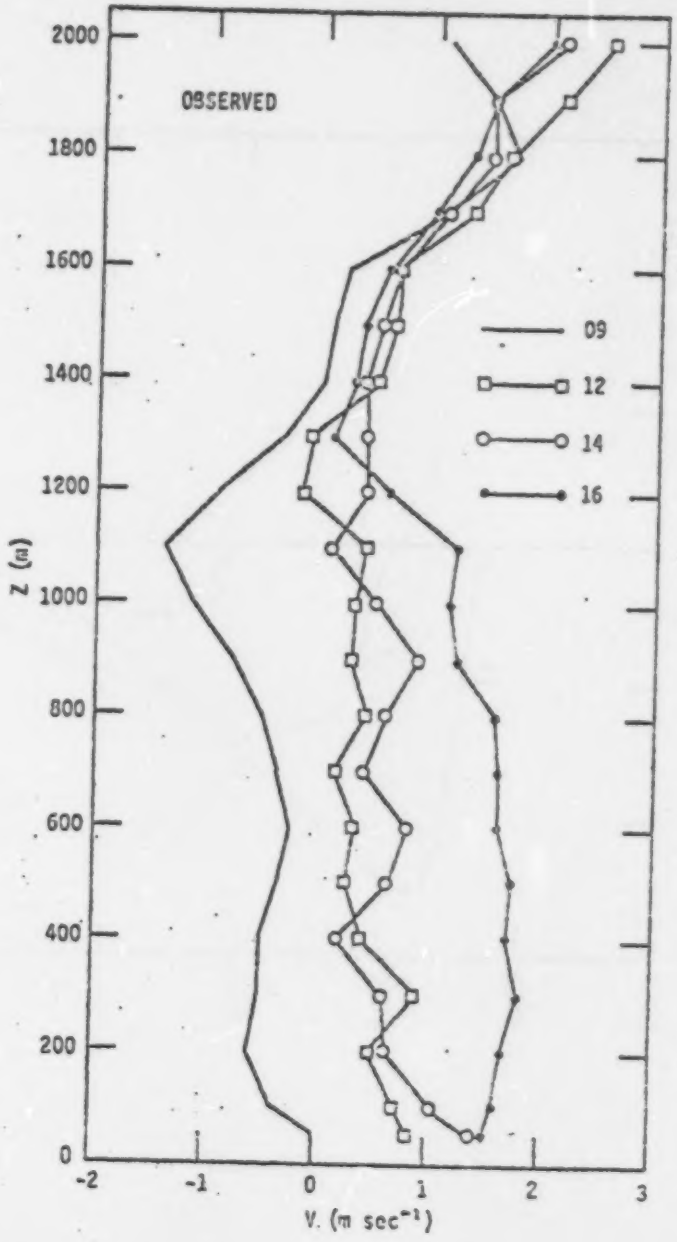
OBSERVED
09
12
14
16
Z (m)
V. (m sec^{-1})

Fig. 6b

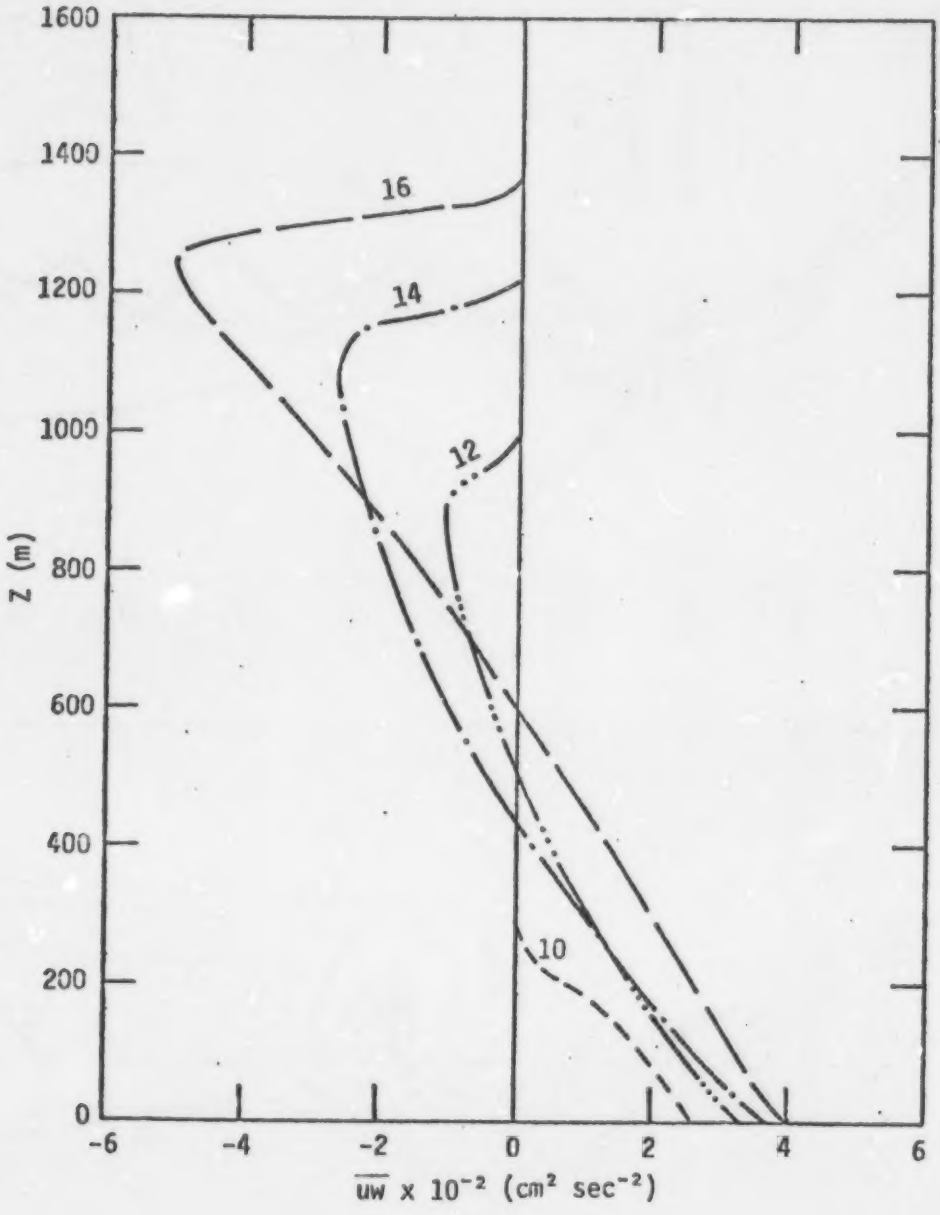
1600
1400
1200
1000
800
600
400
200
0
Z (m)
16
14
12
10
-6
-4
-2
0
2
4
6
$\overline{uw}$ x 10^{-2} (cm^2 sec^{-2})

Fig. 7

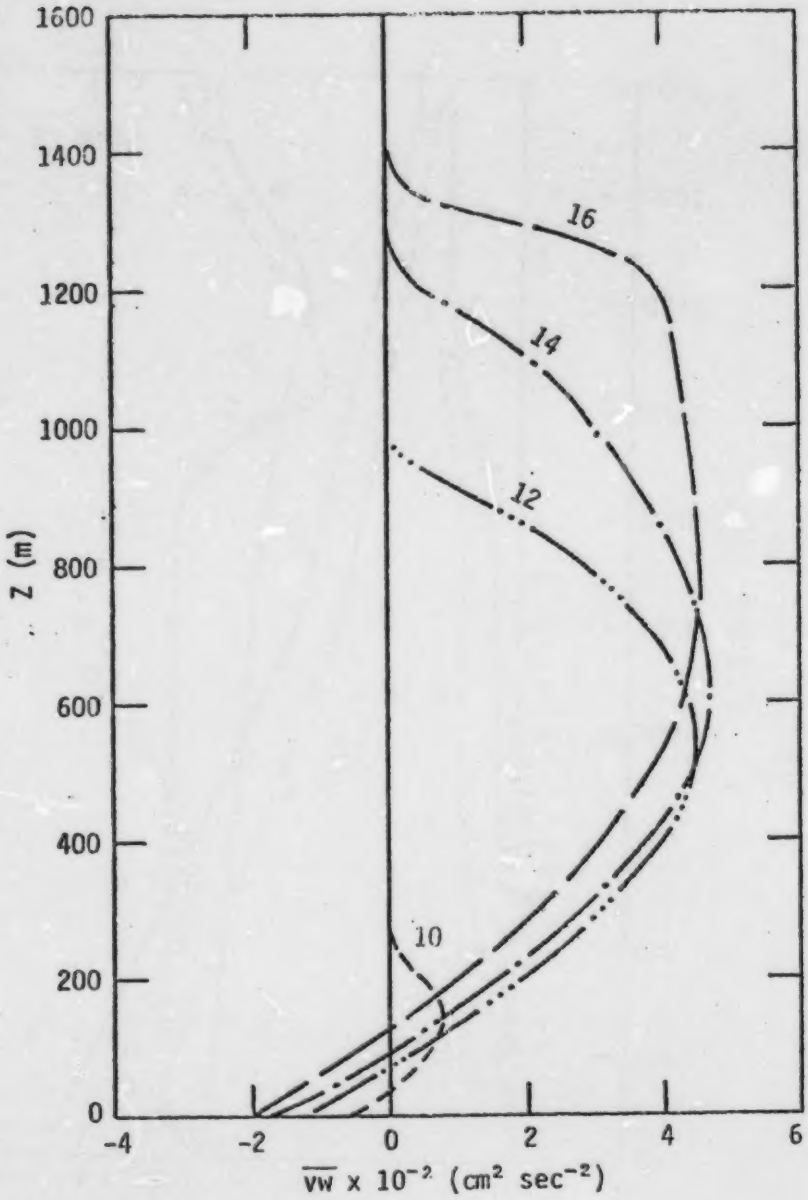
1600
1400
1200
1000
800
600
400
200
0
z (m)
16
14
12
10
-4
-2
0
2
4
6
$\overline{vw}$ x 10^{-2} (cm^2 sec^{-2})

Fig. 8

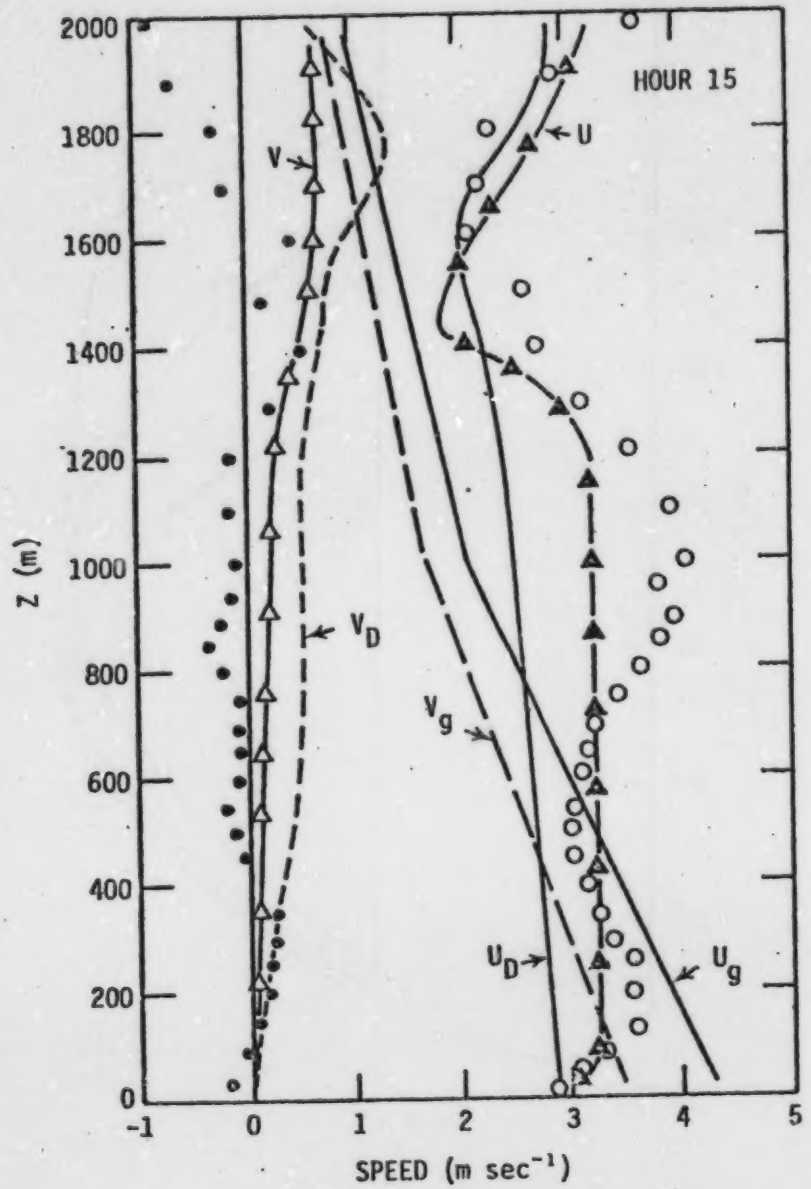
HOUR 15
V
U
V_D
V_g
U_D
U_g
Z (m)
SPEED (m sec^{-1})
2000
1800
1600
1400
1200
1000
800
600
400
200
0
-1
0
1
2
3
4
5

Fig. 9

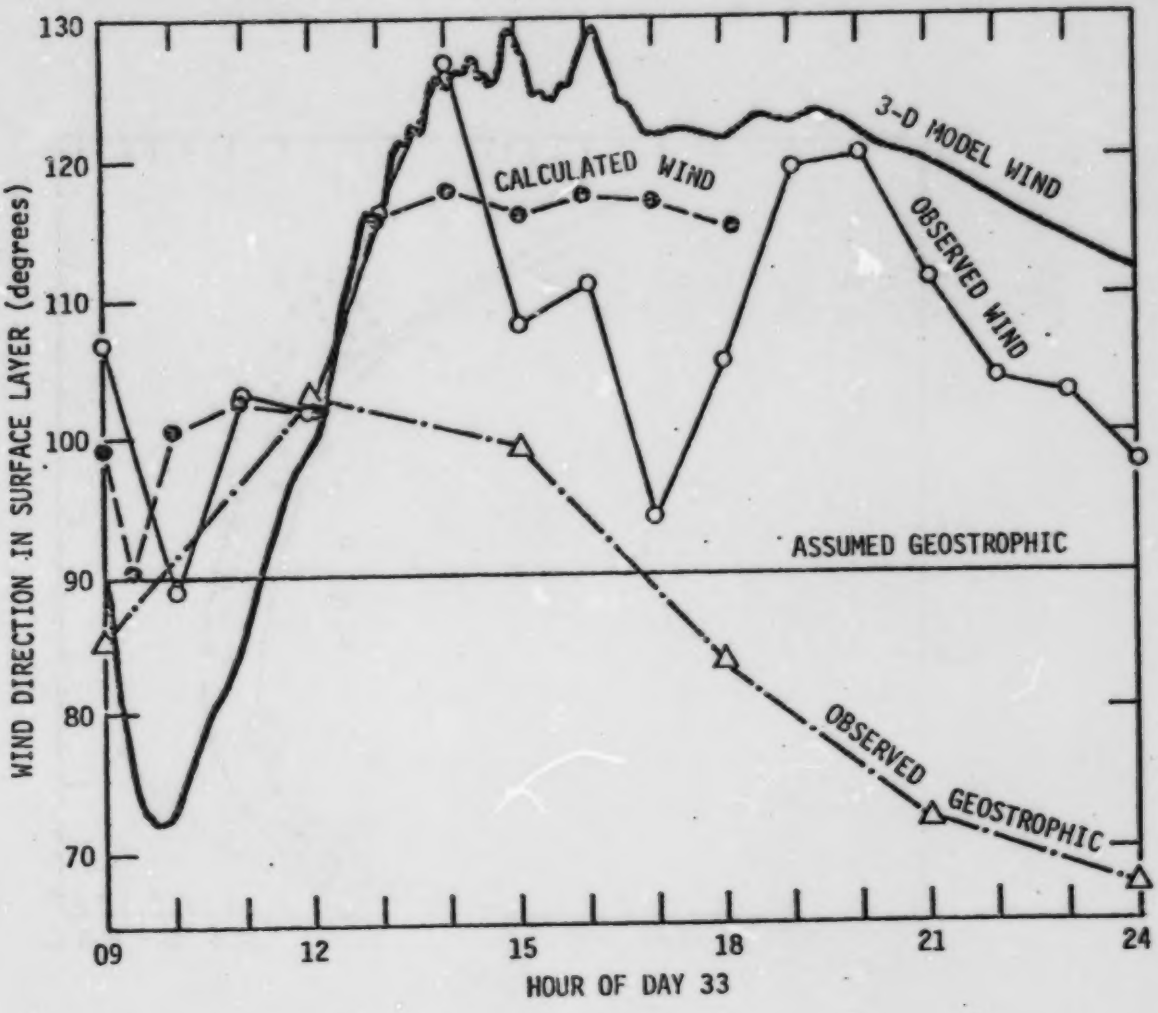
130
120
110
100
90
80
70
WIND DIRECTION IN SURFACE LAYER (degrees)
09
12
15
18
21
24
HOUR OF DAY 33
3-D MODEL WIND
CALCULATED WIND
OBSERVED WIND
ASSUMED GEOSTROPHIC
OBSERVED GEOSTROPHIC

Fig. 10

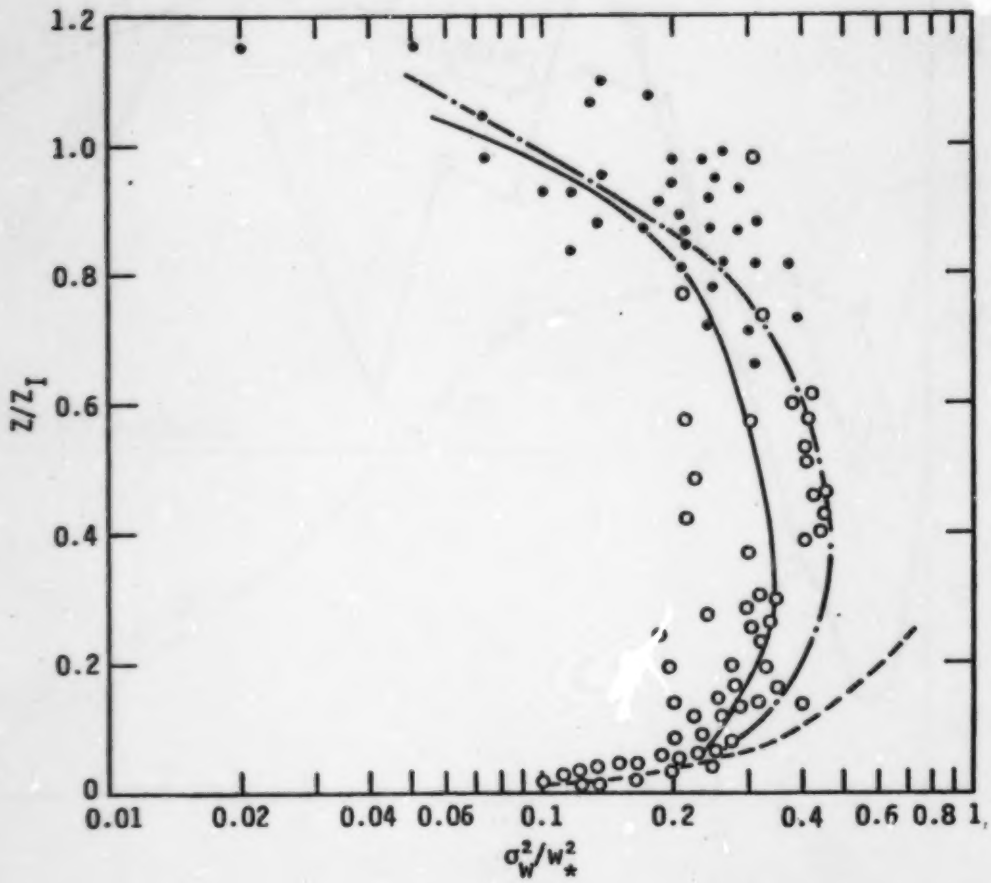

Fig. 11. Vertical velocity variance, σ_w^2, normalized by w_*^2. The solid line is the model prediction at 1400 hours; the dash-dot line indicates the average of the S1 and S2 cases in Willis and Deardorff (1974); the dashed line is the free convection prediction, $\sigma_w^2/w_*^2 = 1.8(z/z_I)^{2/3}$ in Kaimal et al. (1976). The Minnesota and Ashchurch data are shown by open and closed circles respectively.

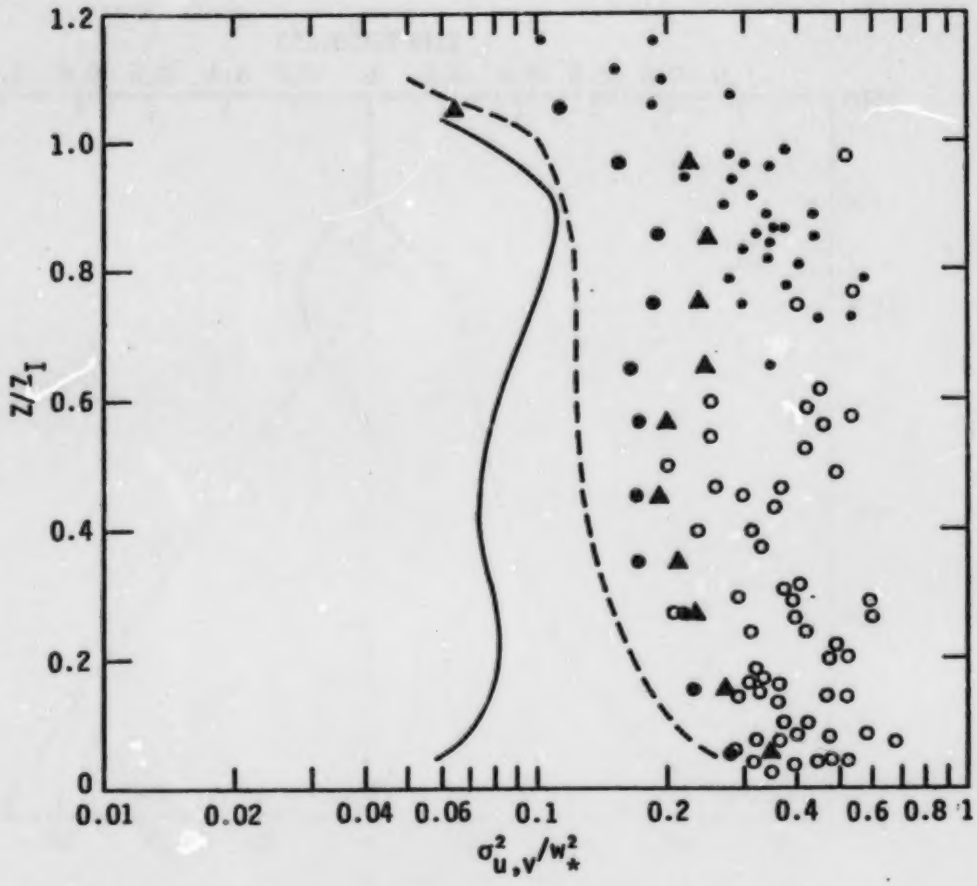

Fig. 12. The average of the horizontal velocity variances, $\sigma^2_{u,v}$, normalized by w^2_*. The solid line is the model prediction at 1400 hours: the dashed line indicates Deardorff's numerical results; large closed circles and triangles represent Willis and Deardorff's results. The Minnesota and Ashchurch data are coded as in Fig. 11.

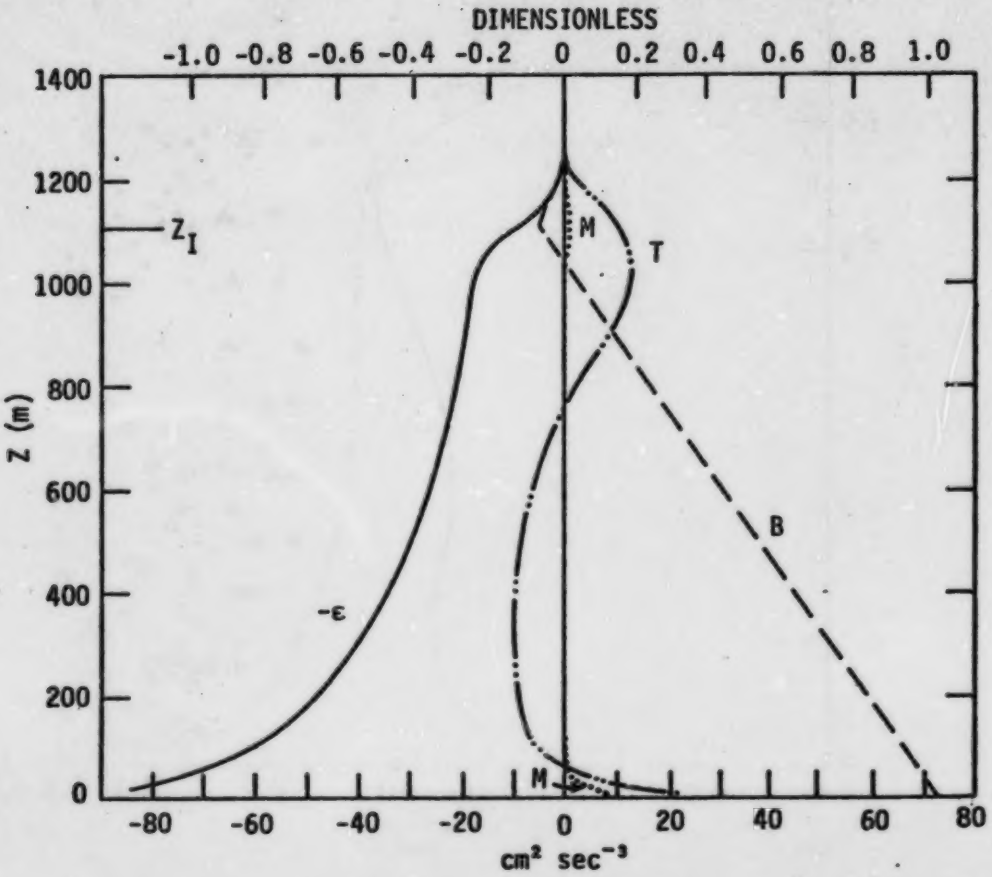

Fig. 13. Eddy kinetic energy budget at 1400 hours; B, buoyant production; M, mechanical (shear) production; - ε, dissipation; T, turbulent transport. The variables are made dimensionless by w_*^3/z_I (= 71.8 cm^2 sec^{-3}).

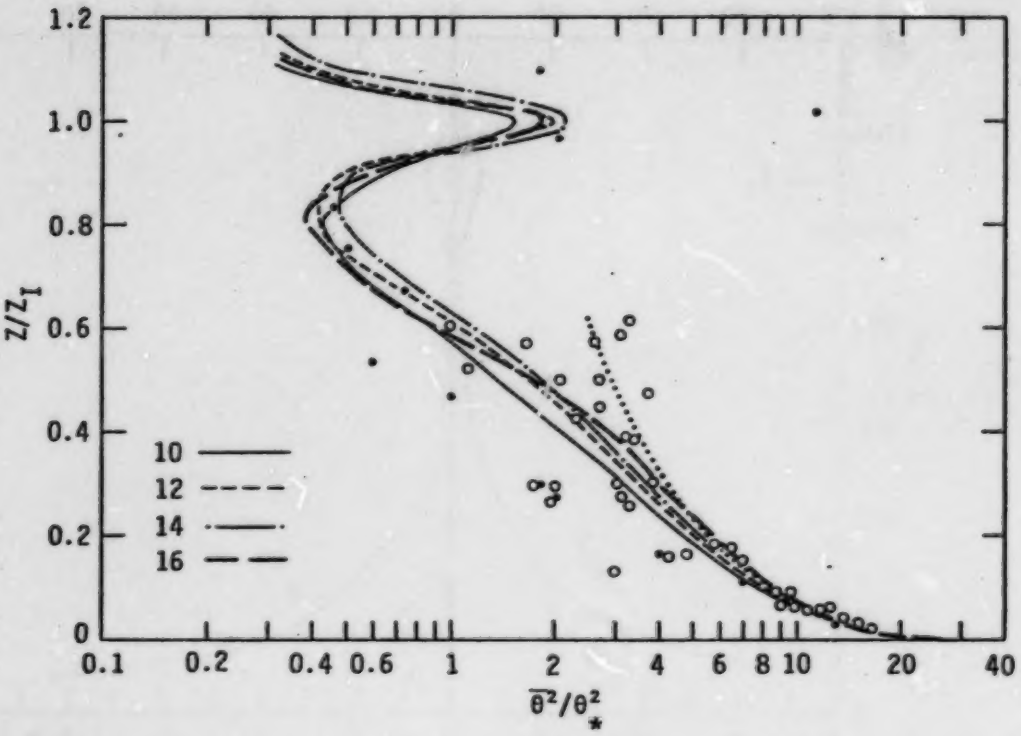

Fig. 14. The normalized temperature variance at various times. The short dashed line represents the free convection prediction, $\overline{\theta}^2/\theta_*^2 = 1.8(z/z_I)^{-2/3}$. Closed circles indicate Willis and Deardorff's results and open circles the Minnesota data.

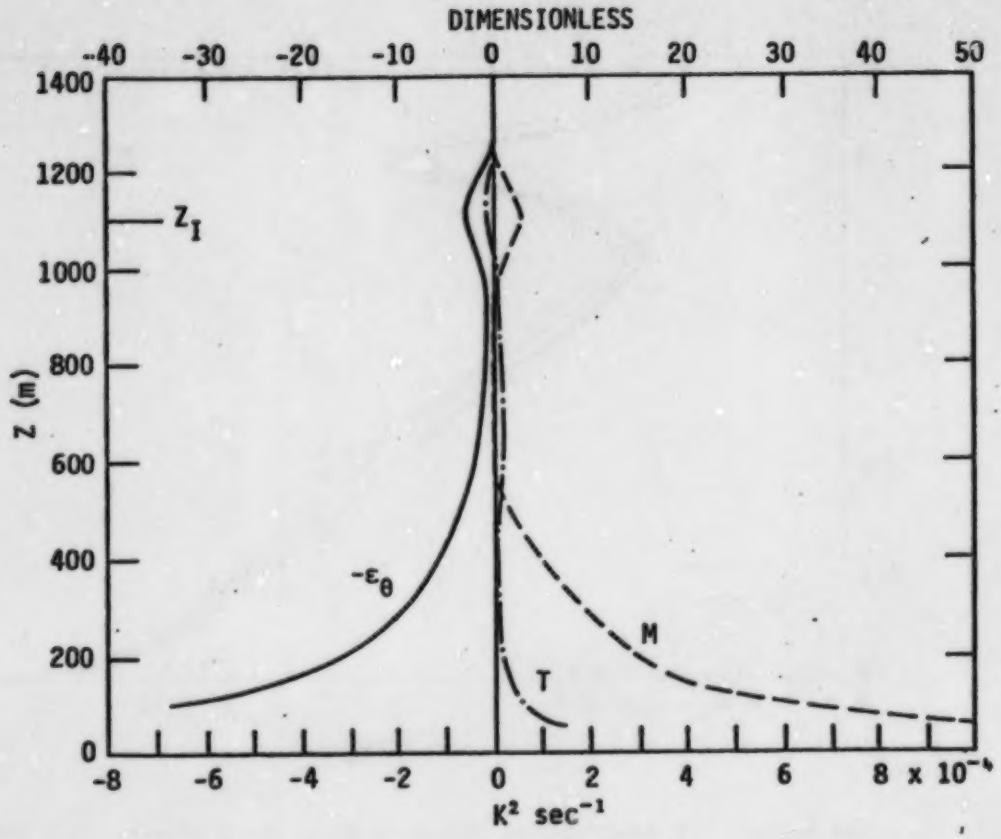

Fig. 15. Virtual potential temperature variance budget at 1400 hours: M, mechanical production; $-\varepsilon_\theta$, molecular destruction; T, turbulent transport. The variables are made dimensionless by $w_*\theta_*^2/z_I$ (= 1.96 x 10^{-5} K^2 sec^{-1}).

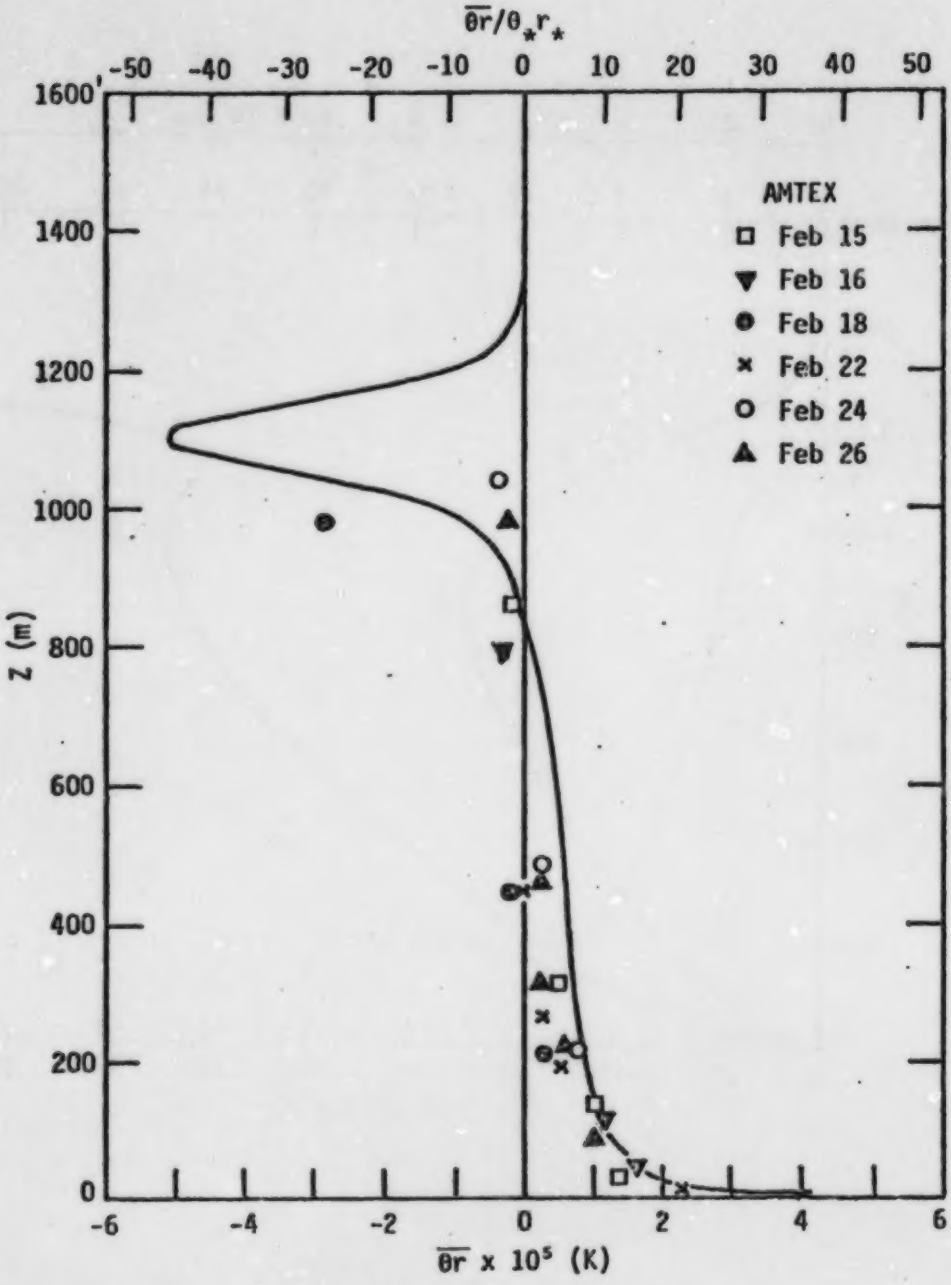
$\overline{\theta r}/\theta_* r_*$
-50 -40 -30 -20 -10 0 10 20 30 40 50
1600
1400
1200
1000
800
600
400
200
0
Z (m)
AMTEX
Feb 15
Feb 16
Feb 18
Feb 22
Feb 24
Feb 26
-6 -4 -2 0 2 4 6
$\overline{\theta r}$ x 10^5 (K)

Fig. 16

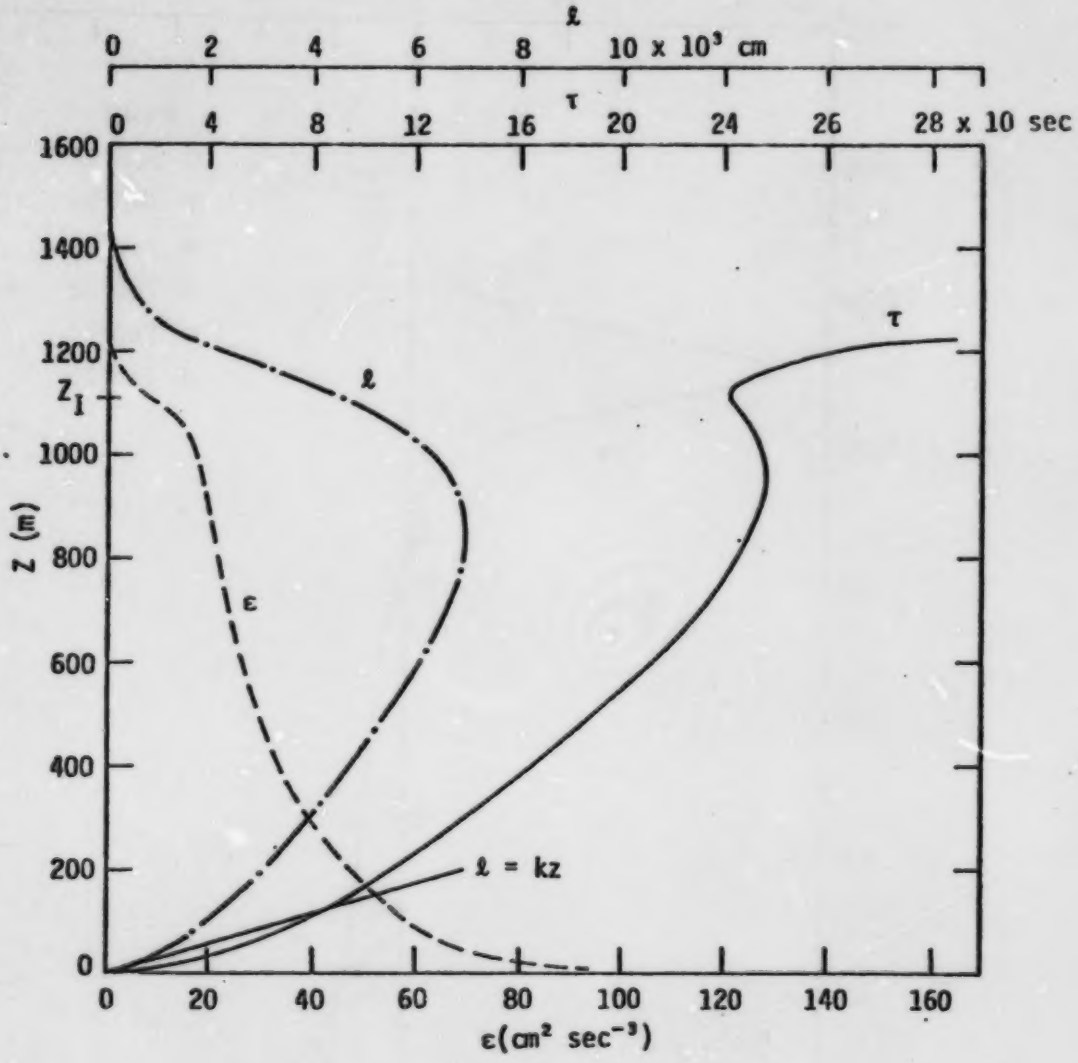
ℓ
0 2 4 6 8 10 x 10³ cm
τ
0 4 8 12 16 20 24 26 28 x 10 sec
1600
1400
1200
Z_I
1000
800
600
400
200
0
Z (m)
ℓ
τ
ε
ℓ = kz
0 20 40 60 80 100 120 140 160
ε(cm² sec⁻³)

Fig. 17

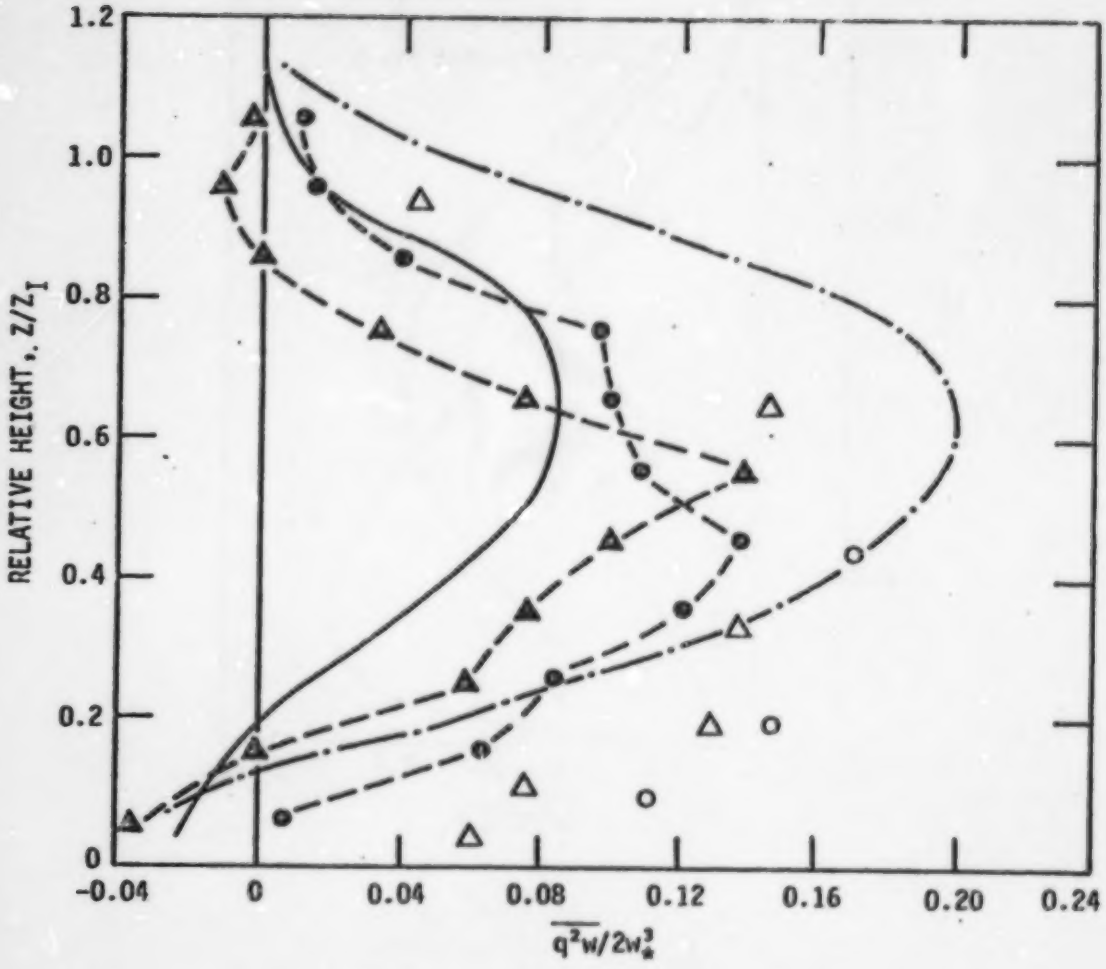
1.2
1.0
0.8
0.6
0.4
0.2
0
RELATIVE HEIGHT, Z/Z_I
-0.04
0
0.04
0.08
0.12
0.16
0.20
0.24
$\overline{q^2w}/2w_*^3$

Fig. 18

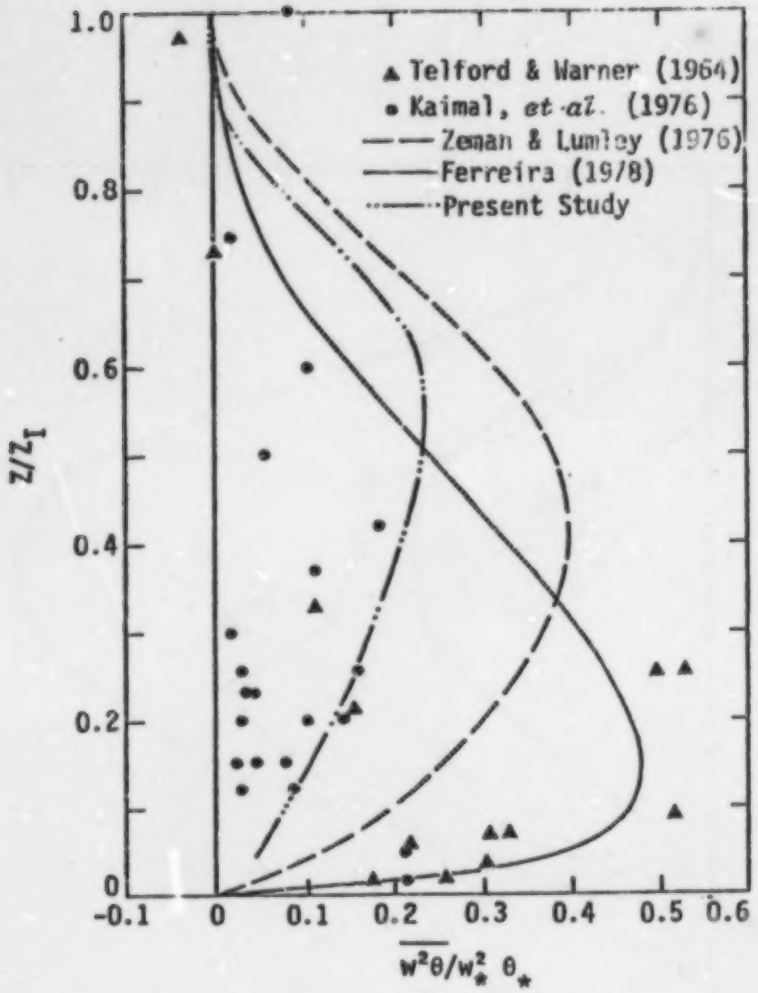
▲ Telford & Warner (1964)
• Kaimal, et al. (1976)
Zeman & Lumley (1976)
Ferreira (1978)
Present Study
1.0
0.8
0.6
0.4
0.2
0
z/z_i
-0.1
0
0.1
0.2
0.3
0.4
0.5
0.6
$\overline{w^2\theta}/w_*^2\,\theta_*$

Fig. 19

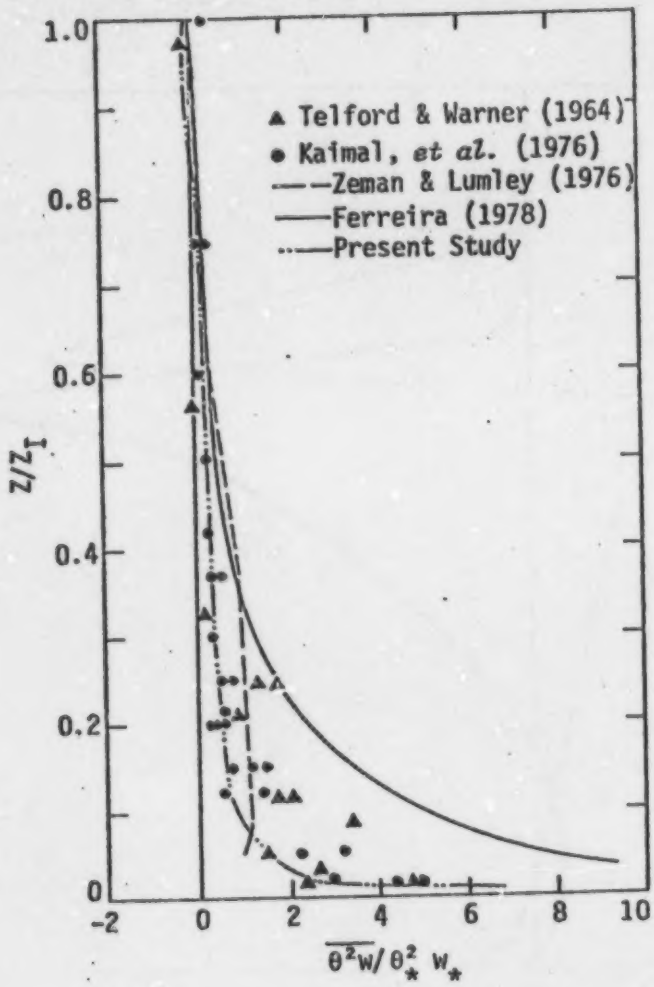
1.0
0.8
0.6
0.4
0.2
0
-2
0
2
4
6
8
10
z/z_i
$\overline{\theta^2 w}/\theta_*^2 w_*$
▲ Telford & Warner (1964)
● Kaimal, *et al.* (1976)
——Zeman & Lumley (1976)
——Ferreira (1978)
·····Present Study

Fig. 20

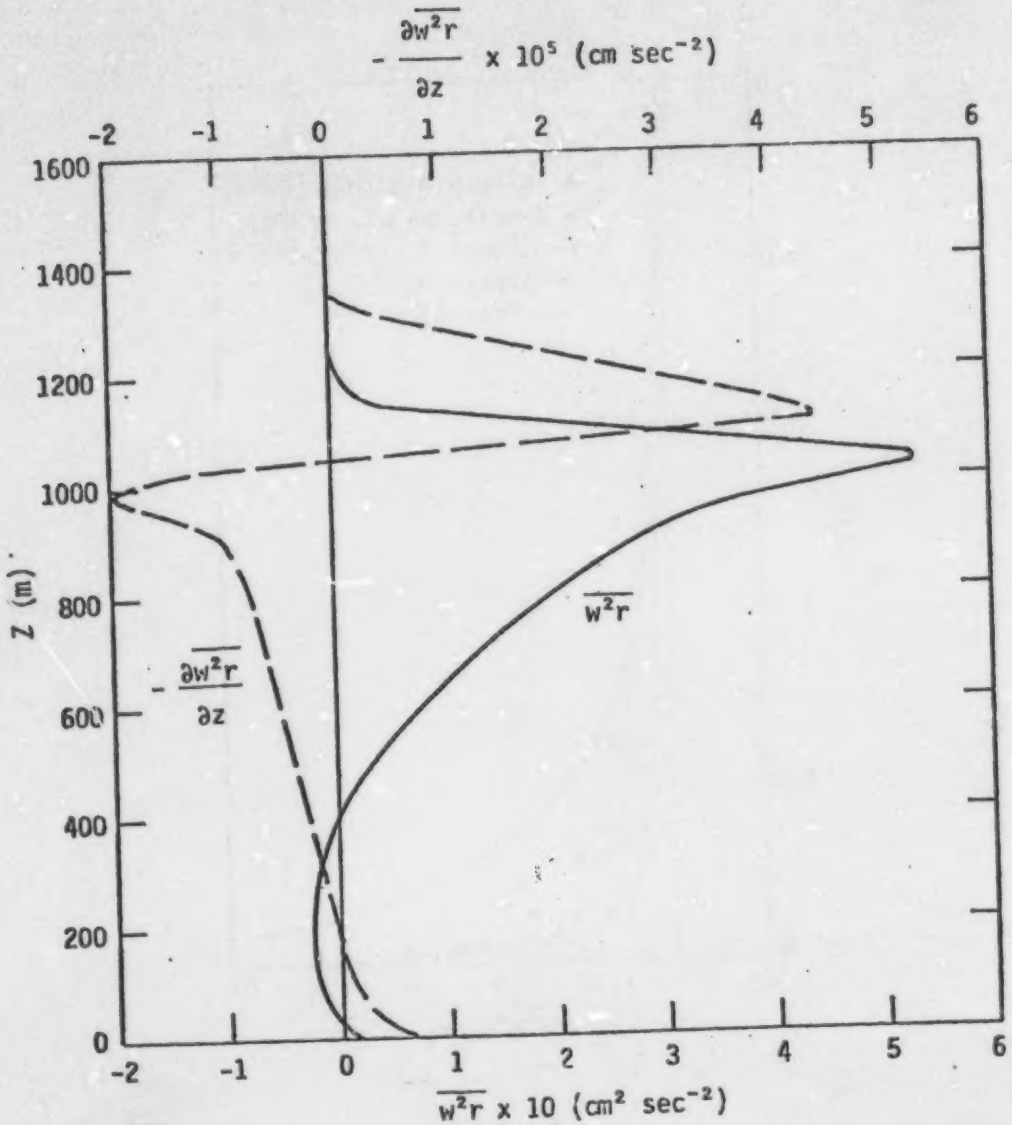
$-\frac{\partial \overline{w^2 r}}{\partial z}$ x 10^5 (cm sec^{-2})
-2
-1
0
1
2
3
4
5
6
1600
1400
1200
1000
800
600
400
200
0
z (m)
$\overline{w^2 r}$
$-\frac{\partial \overline{w^2 r}}{\partial z}$
$\overline{w^2 r}$ x 10 (cm^2 sec^{-2})

Fig. 21